Clonally expanded EOMES+ Tr1-like cells in primary and metastatic tumors are associated with disease progression

Clonally expanded EOMES$^+$ Tr1-like cells in primary and metastatic tumors are associated with disease progression

Raoul J. P. Bonnal[1,2,24], Grazisa Rossetti[1,2,24], Enrico Lugli[3,4,24], Marco De Simone[1,23,24], Paola Gruarin[1,24], Jolanda Brummelman[3,24], Lorenzo Drufuca[1,2], Marco Passaro[1,2], Ramona Bason[1,2], Federica Gervasoni[1,2], Giulia Della Chiara[1,2], Claudia D'Oria[1,2], Martina Martinovic[1], Serena Curti[1], Valeria Ranzani[1], Chiara Cordiglieri[1], Giorgia Alvisi[3], Emilia Maria Cristina Mazza[3], Stefania Oliveto[1], Ylenia Silvestri[1], Elena Carelli[1], Saveria Mazzara[5], Roberto Bosotti[1], Maria Lucia Sarnicola[1], Chiara Godano[1], Valeria Bevilacqua[1], Mariangela Lorenzo[1], Salvatore Siena[6,7], Emanuela Bonoldi[8], Andrea Sartore-Bianchi[6,7], Alessio Amatu[6], Giulia Veronesi[9,10], Pierluigi Novellis[10], Marco Alloisio[11,12], Alessandro Giani[13], Nicola Zucchini[14], Enrico Opocher[15,16], Andrea Pisani Ceretti[15], Nicolò Mariani[15], Stefano Biffo[1,17], Daniele Prati[18], Alberto Bardelli[19,20], Jens Geginat[1,21], Antonio Lanzavecchia[1], Sergio Abrignani[1,21], Massimiliano Pagani[1,2,22]

Affiliations

1 Istituto Nazionale Genetica Molecolare Romeo ed Enrica Invernizzi, Milan, Italy.
2 FIRC Institute of Molecular Oncology (IFOM), Milan, Italy.
3 Laboratory of Translational Immunology, IRCCS Humanitas Research Hospital, Rozzano, Milan, Italy.
4 Flow Cytometry Core, IRCCS Humanitas Research Hospital, Rozzano, Milan, Italy.
5 Division of Hematopathology, European Institute of Oncology (IEO) IRCCS, Milan, Italy.
6 Niguarda Cancer Center, Grande Ospedale Metropolitano Niguarda, Milan, Italy.
7 Department of Oncology and Hemato-Oncology, Università degli Studi di Milano, Milan, Italy.
8 Pathology and Cytogenetics Unit, Grande Ospedale Metropolitano Niguarda, Milan, Italy.
9 Faculty of Medicine and Surgery Vita-Salute San Raffaele University, Milan, Italy.
10 Division of Thoracic Surgery, IRCCS San Raffaele Scientific Institute, Milan, Italy.
11 Division of Thoracic Surgery, IRCCS Humanitas Research Hospital, Rozzano, Milan, Italy.
12 Department of Biomedical Sciences, Humanitas University, Pieve Emanuele, Milan, Italy.
13 Department of Surgery, Milano-Bicocca University, San Gerardo Hospital, Monza, Italy.
14 Department of Pathology, San Gerardo Hospital, Monza, Italy.
15 Unità Operativa Chirurgia Epatobiliopancreatica e Digestiva, Ospedale San Paolo, Milan, Italy.
16 Department of Health Sciences, Università degli Studi di Milano, Milan, Italy.
17 Department of Biosciences, University of Milan, Milan, Italy.
18 Department of Transfusion Medicine and Hematology, IRCCS Ca' Granda Ospedale Maggiore Policlinico, Milan, Italy.
19 Candiolo Cancer Institute, Fondazione del Piemonte per l'Oncologia-IRCCS, Turin, Italy.
20 Department of Oncology, University of Torino, Turin, Italy.
21 Department of Clinical Sciences and Community Health, Università degli Studi, Milan, Italy.
22 Department of Medical Biotechnology and Translational Medicine, Università degli Studi, Milan, Italy.
23 Present address: Department of Radiation Oncology, Cedars-Sinai Medical Center, Los Angeles, CA, USA.
24 These authors contributed equally: Raoul J. P. Bonnal, Grazisa Rossetti, Enrico Lugli, Marco De Simone, Paola Gruarin, Jolanda Brummelman.

Corresponding author

Jens Geginat geginat@ingm.org
Antonio Lanzavecchia lanzavecchia@ingm.org
Sergio Abrignani abrignani@ingm.org
Massimiliano Pagani massimiliano.pagani@ifom.eu

Abstract

Regulatory T (T_{reg}) cells are a barrier for tumor immunity and a target for immunotherapy. Using single-cell transcriptomics, we found that $CD4^+$ T cells infiltrating primary and metastatic colorectal cancer and non-small-cell lung cancer are highly enriched for two subsets of comparable size and suppressor function comprising forkhead box protein $P3^+$ T_{reg} and eomesodermin homolog $(EOMES)^+$ type 1 regulatory T (Tr1)-like cells also expressing granzyme K and chitinase-3-like protein 2. $EOMES^+$ Tr1-like cells, but not T_{reg} cells, were clonally related to effector T cells and were clonally expanded in primary and metastatic tumors, which is consistent with their proliferation and differentiation in situ. Using chitinase-3-like protein 2 as a subset signature, we found that the $EOMES^+$ Tr1-like subset correlates with disease progression but is also associated with response to programmed cell death protein 1–targeted immunotherapy. Collectively, these findings highlight the heterogeneity of T_{reg} cells that accumulate in primary tumors and metastases and identify a new prospective target for cancer immunotherapy.

Main

$CD4^+$ T lymphocytes can provide help to B and $CD8^+$ T cells and coordinate a broad range of antitumor immune responses[1]; however, $CD4^+$ T_{reg} cells can also suppress immune responses thus promoting tumor growth[2]. There is increasing evidence that T_{reg} cells are heterogeneous with characteristic tissue-specific signatures and functions[3,4,5]. Classical $CD4^+$ T_{reg} cells are characterized by expression of the transcription factor forkhead box protein P3 (FOXP3) and maintain tissue homeostasis and tolerance by suppressing self-reactive T cells[6]. However, T_{reg} cells can also infiltrate tumors and their presence is often associated with poor prognosis[7].

Suppression is not limited to $FOXP3^+$ $CD4^+$ T cells. Several studies described $FOXP3^-CD4^+$ T cells, often called Tr1 cells, as endowed with suppressing activity based on the display of cytotoxic functions and production of interleukin-10 (IL-10) that is regulated by BLIMP-1, AhR and c-Maf[8,9,10,11,12,13]. IL-10-producing $FOXP3^-$ Tr1 cells are currently evaluated as a cellular therapy to treat graft-versus-host disease and chronic inflammatory diseases of the gut14. Notably, it was recently reported that a subset of IL-10-producing $FOXP3^-$ Tr1 cells express the transcription factor EOMES[10,12]. Preliminary reports suggest that $FOXP3^-$ Tr1 cells might regulate the antitumor immune response but a molecular characterization of these cells is lacking and the clinical relevance in the tumor microenvironment is unknown[15,16,17].

There is currently great interest in understanding how different effector and regulatory $CD4^+$ T cell subsets shape the tumor microenvironment. The identification of these subsets in tumors is complicated by the plasticity of $CD4^+$ T cells and by the influence exerted by the tissue and tumor microenvironment[18]. Single-cell RNA sequencing (scRNA-seq) provides the opportunity to characterize the immune cell landscape in tissues, unveiling previously undescribed lymphocytes subsets, and can be combined with T cell receptor (TCR) repertoire analysis to define expanded clones and their relationships[19]. This approach has revealed the heterogeneity of intratumoral lymphocytes in non-small-cell lung cancer (NSCLC), melanoma, hepatocellular carcinoma and breast cancer[20,21,22,23]. While providing a broad molecular footprint of immune cells at tumor sites, these studies did not capture the heterogeneity of $CD4^+$ regulatory lymphocytes and their possible relevance in the tumor microenvironment

Here we used scRNA-seq to define the transcriptional identity and TCR repertoire of intratumoral $CD4^+$ T cells in two of the most frequent human tumors, colorectal cancer (CRC) and NSCLC[24]. We found that these tumors and their metastases are highly enriched with both $FOXP3^+$ T_{reg} and $FOXP3^-$ $EOMES^+$ Tr1-like cells. The selective presence of expanded T_{reg} cell clones in tumors suggest that both regulatory populations expand in the tumor microenvironment. Using chitinase-3-like protein 2 (CHI3L2) as a subset signature, we found that enrichment in $EOMES^+$ T_{reg} cells is correlated with disease progression but is also associated with response to anti-programmed cell death protein 1 (PD1).

Results

To characterize the expression signatures and clonal composition of tumor-infiltrating $CD4^+$ T cells, we performed scRNA-seq of $CD4^+$ T cells isolated from two NSCLC and three CRC samples (Supplementary Table

1) using the 5' V(D)J protocol, which provides information on both the TCR and transcriptome of individual T cells (Extended Data Fig. 1). After quality control, we analyzed 25,309 cells, detecting a total of 12,782 unique genes with an average of 1,503 genes per cell. Using the uniform manifold approximation and projection (UMAP) method of visualization, we defined 9 clusters for $CD4^+$ T cells infiltrating NSCLC and 11 clusters for CRC (Fig. 1a and Extended Data Fig. 1a,b). Differential expression analysis performed on the different clusters identified several cluster-specifying genes (Supplementary Table 2) allowing the evaluation of subset conservation across tumors. We used the rank-biased overlap measure[25] to compare the differentially expressed genes (DEGs) of $CD4^+$ T cell clusters in NSCLC and CRC tumors (Fig. 2b) and found that clusters 3 and 4 in CRC displayed the highest similarity with NSCLC clusters 3 and 6, respectively. Cluster 3 in both CRC and NSCLC were characterized by the expression of *FOXP3*, *MAGEH1*, *TIGIT*, *OX40* and *IL2RA*, which are the hallmarks of classical intratumoral T_{reg} cells[26,27]. Interestingly, cluster 4 in CRC and cluster 6 in NSCLC displayed among their top DEGs *EOMES* and *GZMK*, which have been recently described to mark a rare $FOXP3^-$ regulatory subset in peripheral blood and non-tumor tissues[12].

To unequivocally define the $FOXP3^+$ and $EOMES^+$ clusters, we performed a gene set enrichment analysis (GSEA) using reference gene sets previously generated by bulk RNA-seq of human $CD4^+$ T cell subsets[12,26] (Fig. 1c,d) and confirmed that cluster 3 in NSCLC and cluster 3 in CRC were enriched for $CD4^+$ $FOXP3^+$ T_{reg}-specific genes. Importantly, GSEA on cluster 6 in NSCLC and cluster 4 in CRC classified these cells as $EOMES^+$ $FOXP3^-$ Tr1-like cells that have been shown to display several mechanisms of immune suppression[12,14,26]. Consistent results were obtained on 2 additional NSCLC and 3 CRC samples profiled by the Chromium Single Cell 3' protocol for a total of 4 patients with NSCLC and 6 patients with CRC and 40,298 $CD4^+$ T cells analyzed (Supplementary Table 1 and Extended Data Fig. 2a,b). Collectively these findings identify two large subsets of $FOXP3^+$ and $EOMES^+$ CD4 T cells with potential suppressive function, which display the highest similarity across different tumor types.

Characterization of tumor-infiltrating $EOMES^+$ Tr1-like cells

While the detrimental role of $FOXP3^+$ T_{reg} cells in the context of cancer is largely accepted[7,28], there is little information on the role of intratumoral $EOMES^+$ Tr1-like cells. Single-cell transcriptome analysis highlighted *GZMK* as a specific marker of the $EOMES^+$ cluster. To confirm this finding at the protein level, we utilized flow cytometry to assess the coexpression of EOMES and GZMK in tumor-infiltrating $CD4^+$ T cells from 48 patients with NSCLC and 28 patients with CRC and found that in all samples EOMES expression was largely restricted to $GZMK^+$ cells (Fig. 2a and Supplementary Table 3). The $CD4^+$ Tr1-like subset coexpressing EOMES and GZMK lacked the T_{reg} markers CD25 and FOXP3, as well as granulysin (GNLY), a molecule expressed by cytotoxic $CD4^+$ T cells[12], and additionally expressed CCR5 and PD1, two markers of IL-10-producing effector T (T_{eff}) cells[29] (Fig. 2b,c and Extended Data Fig. 3a).

Interestingly, the immunosuppressive cytokine IL-10 was produced exclusively by $EOMES^+$ $GZMK^+$ but not by $EOMES^-$ $GZMK^-$ T cells, together with the effector cytokine interferon-γ (IFN-γ) (Fig. 2d). Furthermore, $EOMES^+$ Tr1-like cells freshly purified from tumors suppressed the proliferation of conventional $CD4^+$ T cells to an extent comparable to that of conventional $FOXP3^+$ T_{reg} cells (Fig. 2e and Extended Data Fig. 3c). Notably, $EOMES^+$ Tr1-like and $FOXP3^+$ T_{reg} cells also strongly suppressed the proliferation of $CD8^+$ T cells, the key effector cells of the antitumor immune response, while control populations containing conventional $CCR5^-$ T_{eff} cells and IL-10-producing $CCR6^+$ helper T cells[30] failed to suppress (Extended Data Fig. 3d). Overall, these findings define an intratumoral $CD4^+$ $EOMES^+$ Tr1-like subset characterized by the expression of GZMK, production of IL-10 and potent suppression of T cell proliferation.

$EOMES^+$ Tr1-like cells are enriched in tumors and metastases

To assess the extent of intratumoral accumulation of $GZMK^+$ $EOMES^+$ T cells, we utilized flow cytometry to analyze permeabilized $CD4^+$ T cells isolated from tumors, adjacent tissue and peripheral blood. In 48 patients with NSCLC and 28 patients with CRC, we found that $EOMES^+$ $GZMK^+$ Tr1-like cells were significantly and selectively increased in tumor tissue (Fig. 3a). The intratumoral accumulation of $GZMK^+$ $EOMES^+$ Tr1-like cells was also documented by tissue staining (Fig. 3b). Furthermore, in both NSCLC and CRC tumors, the percentage of $GZMK^+$ $EOMES^+$ Tr1-like cells was higher in patients with more advanced disease (Fig. 3c). These

findings confirm, at the protein level, the observations made by transcriptomics analysis and indicate an association between intratumoral EOMES$^+$ Tr1-like cells and tumor progression.

In spite of the relevance for cancer progression and disease outcome, the presence of CD4$^+$ T_{reg} cell subsets has not been thoroughly investigated in tumor metastases. Thus, we generated single-cell transcriptomic data from CD4$^+$ T cells isolated from two liver metastases synchronous with the primary CRC lesion (Fig. 3d and Supplementary Table 1). As in primary tumors, we identified two independent clusters of CD4$^+$ T cells characterized by the expression of *FOXP3* and *EOMES* in the metastatic lesions. To perform GSEA analysis on these subsets, we used refined gene set signatures based on 121 genes previously identified from single-cell data of regulatory subsets from primary tumors (Supplementary Table 4). The results of the GSEA analysis showed that EOMES$^+$ Tr1-like and FOXP3$^+$ regulatory cells of primary tumors and metastases share the same molecular blueprints (Fig. 3e).

To further investigate the presence of the two CD4$^+$ regulatory subsets in other tumors, we interrogated publicly available data of scRNA-seq from immune cells infiltrating melanoma, liver and breast tumors and extracted the gene expression data for CD4$^+$ T cells[20,21,22,23]. Using the refined GSEA cell signatures obtained in CRC and NSCLC, we found that the EOMES$^+$ Tr1-like and FOXP3$^+$ T_{reg} cell subsets were enriched in these 3 tumor types, with percentages among total CD4 T cells ranging from 7 to 11% for EOMES$^+$ Tr1-like cells and 7 to 29% for FOXP3$^+$ T_{reg} cells (Fig. 3f,g).

Collectively, these findings indicate that both EOMES$^+$ Tr1-like and FOXP3$^+$ T_{reg} cells are highly enriched in different tumor types and in metastatic lesions, suggesting that they both contribute to suppress immune responses at primary and metastatic sites.

Clonal expansion of regulatory cells in primary and metastatic tumors

To gain an insight into the clonal composition of tumor-infiltrating CD4$^+$ T cells, we recovered paired αβ TCR sequences for 18,615 CD4$^+$ T cells corresponding to 73% of the total cells analyzed from scRNA-seq data (Extended Data Fig. 4a). Using these data, we determined that the clonotype expansion index[31] was highest in the EOMES$^+$ subset (Fig. 4a). Interestingly, all patients with CRC consistently displayed expanded EOMES$^+$ cells with several clonotypes encompassing more than ten cells each (Fig. 4a,b). Clonal expansion of EOMES$^+$ Tr1-like cells was also observed in NSCLC and CRC liver metastases, although with a more heterogenous pattern. Direct comparison of EOMES$^+$ and FOXP3$^+$ repertoires in all tumor types showed that expanded clonotypes (from two to more than ten cells) accounted for approximately half of EOMES$^+$ Tr1-like cells (Fig. 4b and Extended Data Fig. 4b).

To further examine the extent of intraclonal diversification and the clonal composition of different T cell subsets, we evaluated clonotype sharing between EOMES$^+$ Tr1-like or FOXP3$^+$ T_{reg} cells and other CD4$^+$ cell clusters. We found that EOMES$^+$ Tr1-like and FOXP3$^+$ T_{reg} clonotypes were largely confined to their respective subset of origin with little overlap with other clusters. Interestingly, a few expanded EOMES$^+$ Tr1-like clonotypes, and to a lower extent FOXP3$^+$ T_{reg} clonotypes, were also found in other CD4$^+$ clusters as visualized by the Morisita overlap index[32], which provides a quantitative measure of the TCR sequence overlap (Fig. 4c,d). While clonotype sharing was evident for CRC samples and liver metastases, it was less evident for NSCLC. Collectively, the limited overlap between EOMES$^+$ Tr1-like and FOXP3$^+$ T_{reg} clonotypes suggests an independent origin of these two subsets.

In two patients with CRC, we were able to compare the clonotype composition of the primary tumor and synchronous metastasis. In the EOMES$^+$ Tr1-like cluster of the CRC liver metastasis of patient 1, we identified 11 clonotypes that were also found in the primary tumor, 7 in the EOMES$^+$ cluster and 4 in other FOXP3$^+$ clusters. In addition, within the FOXP3$^+$ T_{reg} cluster of the liver metastasis, we identified four clonotypes of which three were found in the FOXP3$^+$ T_{reg} cluster of the primary tumor and one in other EOMES$^+$ Tr1-like clusters (Fig. 4e). In the EOMES$^+$ Tr1-like cluster of the liver metastasis of patient 2, we identified a high number of clonotypes shared with the primary tumor—81 clonotypes in the EOMES$^+$ cluster, 1 in the FOXP3$^+$ cluster and 39 in other clusters. In the FOXP3$^+$ T_{reg} of this metastasis, we identified 59 clonotypes shared with the FOXP3$^+$ cluster of the primary tumor and 3 clonotypes shared with other non-EOMES$^+$ clusters (Fig. 4e and Extended Data Fig. 4c). Collectively, these findings are consistent with an

independent clonal expansion of the two regulatory subset, which is possibly driven by recognition of antigens shared by primary and metastatic tumors.

The TCR sequence overlap between EOMES$^+$ Tr1-like cells and other clusters suggests that intratumoral EOMES$^+$ Tr1-like cells might differentiate from conventional CD4$^+$ T cells in situ. Thus, we used GSEA to define the identity of the clusters with the highest clonotype sharing with EOMES$^+$ Tr1-like cells as determined by the Morosita overlap index in samples of CRCs and liver metastases (Fig. 4f). This analysis, which was not performed on NSCLC due to the limited sample size, showed that cluster 6 in CRC and cluster 1 in liver metastases were enriched for type 1 helper T (T_H1)-like cells (Fig. 4f). In line with this observation, we performed in vitro experiments to induce EOMES expression in antigen-experienced CD4$^+$ T cells and found that T_H1 cells were the only subset that could upregulate EOMES in vitro (Fig. 4g). T_H1 cells isolated form peripheral blood upregulated EOMES in the presence of IL-4, while IL-12 and IL-27 had no effect at all (Fig. 4g and Extended Data Fig. 5a). Intriguingly, EOMES induction in T_H1 cells was less effective with CD28 co-stimulation (Fig. 4g), a finding that is consistent with the observation that antigen-experienced T cells upregulate EOMES in response to immature dendritic cells but less efficiently to mature dendritic cells (Extended Data Fig. 5b). Moreover EOMES$^+$ Tr1-like cell lines maintained EOMES and GZMK expression and IL-10 producing capacity and suppressive function for several months, although in vitro cultures did not fully recapitulate the more complex conditions that shape the identity of these cells in vivo (Extended Data Fig. 5c,d). Overall, these data suggest that EOMES$^+$ Tr1-like cells are terminally differentiated cells that may derive from T_H1 cells in the tumor microenvironment.

CHI3L2 expression marks EOMES$^+$ Tr1-like cells

To assess the possible contribution of EOMES$^+$ Tr1-like cells to disease outcome, we searched for a transcript that would selectively identify the EOMES$^+$ Tr1-like subset among all other cell types of the tumor environment. We first analyzed all the CD4$^+$ T cell datasets we generated in patients with NSCLC and CRC (Fig. 1b) and identified the 12 most selectively expressed genes in EOMES$^+$ Tr1-like cells, which include the gene encoding CHI3L2, a secreted protein belonging to a family of chitinase-like proteins with growth factor activity on cells of tumor and non-tumor origin[33]. To validate the cell specificity of these 12 markers across all other cell types present in the tumor microenvironment (besides CD4$^+$ T cells) we assessed their expression on 23 CRC scRNA-seq datasets comprising all cells found in the tumor ecosystem[34] (Fig. 5a). The results shown in Fig. 5b show that CHI3L2 stands out as a preferential marker for CD4$^+$ EOMES$^+$ T_{reg} cells. Since single-cell data are sparse, especially for low-expressed genes, we employed quantitative PCR with reverse transcription (RT–qPCR), to further validate the relative expression of *CHI3L2* in different lymphocyte subsets (EOMES$^+$ Tr1-like cells, CD8 T cells, natural killer (NK) cells, B cells and whole CD4$^+$ T cells depleted of EOMES$^+$ cells) isolated from NSCLC and CRC tumors as well as in whole tumors and adjacent tissues depleted of the immune cell components (Fig. 5c). Collectively, these findings demonstrate that *CHI3L2* is upregulated in EOMES$^+$ Tr1-like cells and can therefore serve as a marker of these cells.

Using *CHI3L2* as a tag for EOMES$^+$ Tr1-like cells, we reanalyzed a large transcriptomic dataset of whole resected tissues from a cohort of 177 patients with CRC, 80 patients with NSCLC and 103 patients with melanoma[35,36] and reassessed the survival rate in high and low *CHI3L2*-expressing tumors (Fig. 5d). Remarkably, patients bearing tumors with high levels of *CHI3L2* expression had a shorter survival compared to patients whose tumors expressed low levels of *CHI3L2*. We also performed multivariate analysis to determine whether expression of *CHI3L2* was associated with mortality relative to other risk factors and found that the hazard of death still correlated with high *CHI3L2* expression even when other covariates such as age, sex and tumor stage were taken into account (Extended Data Fig. 6a). Overall, we conclude that in this patient series high expression of *CHI3L2*, as marker of EOMES$^+$ Tr1-like cells, is an independent predictor of patient survival for these three tumor types.

Infiltration of immune cells in the tumor microenvironment has been associated with response to immunotherapy[37] but there is only limited information on the effect of tumor-infiltrating regulatory subsets on the response to immune checkpoint inhibitors[28]. Thus, after confirmation that *CHI3L2* can be exploited as a proxy for EOMES$^+$ Tr1-like cells in melanoma[22] (Extended Data Fig. 6b), we interrogated whole-transcriptome data generated on melanoma samples from a cohort of patients before anti-PD1/programmed cell death 1 ligand 1 (PD-L1) treatment[38]. Interestingly, high expression of *CHI3L2* and, to a lesser degree, expression

of *FOXP3* or *CCR8* independently correlated with a prolonged progression-free survival after immunotherapy (Fig. 5e and Extended Data Fig. 6e). We then asked whether PD1 blockade could affect EOMES$^+$ Tr1-like cell function and we found that the capacity of EOMES$^+$ T_{reg} cells to suppress the proliferation of antigen-experienced CD8$^+$ T cells is reduced in the presence of anti-PD1 antibodies (Fig. 5f). Collectively, these data indicate that the response to immune checkpoint inhibitors is a characteristic of tumors highly infiltrated with suppressive cells comprising both classical FOXP3$^+$ T_{reg} and EOMES$^+$ Tr1-like cells.

Discussion

Using an unbiased single-cell transcriptome analysis, we assessed the heterogeneity of intratumoral CD4$^+$ T cells in six different tumor types (NSCLC, CRC, melanoma, liver, breast cancer and liver metastasis) and found that all tumors are highly enriched with two distinct subsets of comparable size and suppressive function: the classical FOXP3$^+$ T_{reg} and IL-10-producing EOMES$^+$ Tr1-like cells.

IL-10-producing CD4$^+$ T cells with suppressive function (Tr1) were discovered more than 20 years ago both in mice and man[39]. The initial work focused on the characterization of T cell clones since their frequency in peripheral blood mononuclear cells is very low. Further work demonstrated that IL-10 can also be produced by most T_{eff} cells depending on the nature of the priming antigen and on the timing and conditions of in vitro stimulation[40,41]. These findings led to the proposition that IL-10 production may define a functional state of CD4$^+$ T cells rather than a distinctive population. A better definition of a Tr1 subset came from the identification of surface markers[11] and of the selective expression of EOMES[12]. Using an unsupervised approach, we identified EOMES$^+$ Tr1-like cells as a major intratumoral population characterized by the expression of GZMK and granzyme A, capable of producing IL-10 and IFN-γ and of suppressing T cell proliferation in vitro. Tr1 cells have been shown to transdifferentiate from T_H17 cells during resolution of inflammation. Our TCR clonality data do not support this pathway in the tumor microenvironment[42]. The precise relationship between the rare, heterogenous IL-10-producing Tr1 cells in peripheral blood and the prominent population of clonally expanded intratumoral EOMES$^+$ Tr1-like cells with a distinctive gene signature is to be established.

The high proportion of EOMES$^+$ Tr1-like cells (7–15% of CD4$^+$ T cells) and of classical FOXP3$^+$ T_{reg} cells in tumors (7–29%) is consistent with the notion that the tumor microenvironment can attract and nurture T cells that play a role in tissue repair and homeostasis, thus benefitting the tumor[3,43]. Furthermore, the high frequency of expanded clones suggests that the two regulatory subsets proliferate in the tumor microenvironment, possibly in response to tumor antigens.

The observation that there was little or no overlap of TCR clonotypes between FOXP3$^+$ T_{reg} and EOMES$^+$ Tr1-like cells suggests a complementary, rather than redundant, role. Furthermore, the finding of expanded T_{reg} clonotypes shared between primary CRC and synchronous liver metastases suggest an independent clonal expansion driven by antigens shared by the primary and metastatic tumors. Finally, the identification of certain EOMES$^+$ Tr1-like cell clonotypes also found in other CD4$^+$ T cell subsets is consistent with some degree of functional plasticity of CD4$^+$ T cell subsets[44,45]. We cannot exclude that additional T_{reg} cell populations may be present in certain tumors.

Previous studies using bulk and scRNA-seq identified a unique signature in intratumoral FOXP3$^+$ T_{reg} cells with selective expression of *CCR8*, *MAGEH1* and *LAYN1* (refs. [20,21,22,23,26,27,46]) but failed to identify EOMES$^+$ Tr1-like cells. Other studies based on the analysis of infiltrating T cells suggested the existence of FOXP3$^-$ T cells with suppressing activity but these cells were poorly characterized and thought to represent a minor and heterogeneous population[15,16,17]. By restricting the analysis on CD4$^+$ T cells, we were able to use *EOMES* as a selective marker of the FOXP3$^-$ Tr1-like subset, which could be otherwise misclassified due to the high expression of *EOMES* also in CD8 T cells[47,48]. This strengthens the relevance of *CHI3L2* transcript expression for the correct identification of EOMES$^+$ Tr1-like cells in the tumor microenvironment. *CHI3L2* encodes a secreted protein belonging to a family of chitinase-like proteins that lack chitinase activity but have growth factor activities[49]. It is interesting that a close member of the chitinase-like proteins, CHI3L1, has been reported to enhance inflammatory responses and promote tumor growth[50].

Using *CHI3L2* as a marker of EOMES$^+$ Tr1-like, we could assess the prognostic relevance of this subset for the survival of patients with NSCLC, CRC or metastatic melanoma. The observed correlation between high

expression of *CHI3L2* and worst prognosis suggests that EOMES$^+$ Tr1-like cell accumulation favors tumor progression through mechanisms that have to be determined but may be related to direct pro-tumor effects or to the suppression of the antitumor effector response. Interestingly, in a cohort of patients with metastatic melanoma treated with anti-PD1/PD-L1 antibodies[38], a higher number of EOMES$^+$ regulatory cells, inferred by *CHI3L2* expression levels, were associated with a better response to immunotherapy. Indeed, anti-PD1 seems to decrease the EOMES$^+$ Tr1-like cells suppressive function in vitro, even if the underlying mechanism in vivo is to be elucidated. These findings, together with the high expression of PD1 on both FOXP3$^+$ T_{reg} and EOMES$^+$ Tr1-like cells, suggest that both T_{reg} subsets are direct targets of immunotherapy.

Overall, our findings support the hypothesis that EOMES$^+$ T_{reg} cells contribute, in concert with FOXP3$^+$ T_{reg} cells, to the establishment of a suppressive tumor microenvironment, which is very conserved across tumor types. Consequently, both should be targeted by combined and new immunotherapeutic strategies to effectively boost specific antitumor immune responses in a wide array of cancers including metastatic lesions.

Methods

Human primary tissues

Primary tumors and nonneoplastic counterparts were obtained from surgical resection of thirty-four CRCs and fifty-two NSCLCs. Informed consent was obtained from all patients and the study was approved by the institutional review board of the San Gerardo Hospital, San Paolo Hospital, Grande Ospedale Metropolitano Niguarda and Humanitas Research Hospital (protocol no. 1501). No patients received palliative surgery or neoadjuvant chemotherapy and/or radiotherapy. NSCLC specimens and adjacent tumor-free tissues were cut into pieces and single-cell suspensions were prepared using the Tumor Dissociation Kit, human (catalog no. 130-095-929; Miltenyi Biotec) and the gentleMACS Dissociator (catalog no. 130-093-235; Miltenyi Biotec). Cell suspensions were then resuspended in dimethylsulfoxide with 10% FCS and stored in liquid nitrogen until flow cytometry or processed further by Ficoll-Paque density gradient centrifugation (Amersham Bioscience). CRC specimens were cut into pieces, incubated in 1 mM of EDTA (Sigma-Aldrich) for 50 min at 37 °C and then incubated in type D collagenase solution 0.5 mg ml^{-1} (Roche Diagnostic) for 4 h at 37 °C.

Cell preparation

Mononuclear cells were isolated from cell suspensions by Ficoll-Paque density gradient centrifugation. T cell fractions were recovered after fractionation on a four-step gradient consisting of 100, 60, 40 and 30% Percoll solutions (Pharmacia). EOMES$^+$ CD4$^+$ T_{reg} cells were purified by flow cytometry sorting using the following fluorochrome conjugated antibodies: anti-CD4 APC/Cy7 0.5 µl 10^{-6} cells (clone OKT4; BioLegend); anti-IL-7R PE 1 µl 10^{-6} cells (clone MB15-18C9; Miltenyi Biotec); anti-CD25 VioBright FITC 0.5 µl 10^{-6} cells (clone 4E3; Miltenyi Biotec); anti-CD27 VioBlue 1 µl 10^{-6} cells (clone M-T271; Miltenyi Biotec); anti-CD195 PEcy7 1 µl 10^{-6} cells (clone J418F1; BioLegend) using a FACSAria II (BD Biosciences) with BD Biosciences proprietary software as CD4$^+$IL-7R$^-$CCR5$^+$CD27$^+$ (Extended Data Fig. 3b)[12]. Fresh cells were collected, washed with PBS and resuspended in PBS supplemented with 0.04% BSA. Cell were then counted using an automated counter (Countess II; Thermo Fisher Scientific) and cell viability was assessed by Trypan blue exclusion. Samples were selected according to cell viability; for the analysis, samples with a viability >85% were used.

Flow cytometry

Cytokine production was assessed by intracellular staining after stimulation with 0.1 µM of phorbol-12-myristate-13-acetate (PMA) and 1 µg ml^{-1} of ionomycin (Sigma-Aldrich) in the presence of 10 µg ml^{-1} of brefeldin A (Sigma-Aldrich). Intracellular staining was performed using the eBioscience FOXP3 staining kit according to the manufacturer's protocol (catalog no. 00-5523-00). Briefly, cells were collected and fixed for 30 min in fixation/permeabilization buffer at 4 °C and then stained with anti-EOMES antibody eFluor 660 1:50 (clone WD1928; eBioscience), anti-IL-10PE 1:25 (clone JES-19F1; BioLegend), anti-IFN-γ PerCP/Cy5.5 1:100 (clone 4S.B3; BioLegend), anti-granzyme K FITC 1:50 (clone GM6C3; Santa Cruz Biotechnology) in permeabilization buffer for 30 min at 4 °C. Cells were then washed two times, resuspended in FACS washing buffer and analyzed by flow cytometry.

Sequencing library construction using the Chromium 10x platform

Cellular suspensions (5,000 or 10,000 cells per sample) were loaded on a Chromium 10x Instrument (10x Genomics) to generate single-cell gel beads in emulsion. scRNA-seq libraries were prepared using the Chromium Single Cell 3' or Chromium Single Cell 5' Library Construction Kit according to the manufacturer's instructions. Sequencing libraries were loaded on an Illumina HiSeq 2500 or NovaSeq platform and sequenced at 50,000 reads per cell for gene expression analysis and 5,000 reads per cell for TCR analysis.

scRNA-seq data processing and quality control

The FASTQ files of tumor-infiltrating $CD4^+$ cells were processed by the Cell Ranger software pipeline v.3.0.1 provided by 10x Genomics using default parameters, creating a raw count matrix for each analyzed sample. Each matrix was then processed using the Python package SCANPY v.1.4.2 (ref. [51]). First, cells with fewer than 200 expressed genes and genes detected in less than 0.1% of the total sample cells and cells with fewer than 200 expressed genes were removed. Low-quality cells and outliers based on the percentage of mitochondrial and ribosomal genes, total number of genes and gene counts were detected according to the median absolute deviation (MAD)[52]. Cells were removed if the value of any of the above features was greater than the number of selected MAD above the median.

After filtering, the remaining data were concatenated according to tumor type and sequencing protocol, yielding the final matrices used for the downstream analysis. Concatenated matrices were then normalized using a scaling factor of 10^4 and log-transformed using scanpy.pp.normalize_per_cell(data, counts_per_cell_after = 1e4) and scanpy.pp.log1p(data), respectively. Within each batch, highly variable genes (HVGs) were selected based on specific thresholds for mean expression and dispersion using scanpy.pp.highly_variable_genes(min_mean = 0.08, max_mean = 4, min_disp = 0.7) and excluding mitochondrial and ribosomal genes. Only HVGs common to all batches were retained to smooth out batch-related variability.

Dimensionality reduction and clustering

Principal component analysis was performed on scaled and centered values considering selected HVGs. Unwanted sources of variation (that is, number of detected counts and genes per cell, percentages of mitochondrial and ribosomal counts and cell cycle phase) were evaluated and regressed out using a linear regression as implemented in SCANPY (scanpy.pp.regress_out). Furthermore, possible batch effects were corrected using the ComBat algorithm (https://scanpy.readthedocs.io/en/stable/api/scanpy.pp.combat.html). Then, a *k*-nearest neighbor graph was constructed based on Euclidean distance in principal component analysis space, considering a limited number of principal components. Finally, the Leiden algorithm was used to perform unsupervised clustering of cells (scanpy.tl.leiden).

Data visualization and trajectory analysis and identification of differential expression genes

UMAP was used to visualize the data[53]. The number of principal components used to calculate the embedding were the same as those used for the clustering. DEGs for each cluster against all other clusters were identified using scanpy.tl.rank_genes_groups implemented by SCANPY with default parameters. Leiden-defined clusters were labeled by manual inspection of marker genes. Upregulated DEG lists were used as ranked gene lists to perform GSEA. Signature gene lists are reported in Supplementary Table 2.

Definition of gene descriptors for $CD4^+$ $EOMES^+$ Tr1-like cells within $CD4^+$ T cell datasets and the whole tumor ecosystem

Within each $CD4^+$ T cell scRNA-seq dataset, the best gene descriptors for $CD4^+$ $EOMES^+$ T_{reg} cells were defined as genes with a fold change >5 and $P < 0.01$ in at least 70% of comparisons when comparing $CD4^+$ $EOMES^+$ T_{reg} cells with all other clusters individually. Marker selection was subsequently refined by intersecting the list derived from all NSCLC and CRC available datasets. The resulting gene list was then projected on scRNA-seq datasets from 23 CRC samples to assess their expression across all cell clusters present in the tumor environment.

GSEA

GSEA was performed by pre-ranked GSEA[54] using the custom genes modules we previously generated[26] and the prerank() function implemented in the gseapy v.0.9.13 package. For clusters of interest, genes were ranked according to the score computed by the rank_genes_groups() function implemented in the SCANPY tools module with default parameters. The refined gene set for FOXP3$^+$ T_{reg} and EOMES$^+$ Tr1-like subsets was defined by the intersection of the DEGs for both clusters in CD4$^+$ T cell scRNA-seq datasets from both CRC and NSCLC. The two resulting gene lists comprised 121 genes each (Supplementary Table 4).

TCR analysis

After cluster analysis, in-depth analysis of TCR clonality was performed. Initially, cells were paired with proper clonotypes as reconstructed by the Cell Ranger pipeline. Clonotypes were encoded as a collection of semicolon-separated (chain: cd3r_sequence) pairs for each reconstructed chain. Only cells associated with a standard productive TCR (α and β chains) were retained. Clonal expansion within clusters was evaluated using the EXPA index as defined in the STARTRAC package v0.1.0 (https://github.com/Japrin/STARTRAC). The Morisita–Horn similarity index was used to probe the similarity between the TCR repertoire across clusters. This unitless index takes into account the number of shared sequences between two repertoires as well as the contribution of those shared sequences to each repertoire.

Total RNA isolation and RT–qPCR

Total RNA was isolated using the TRIzol Reagent (Thermo Fisher Scientific) according to the manufacturer's instructions. Residual contaminating genomic DNA was removed from the total RNA fraction using the DNA-*free* Kit (Thermo Fisher Scientific). RNA yields were quantified using the QuantiFluor RNA System (Promega Corporation) with Quantus Fluorometer (Promega Corporation); RNA quality was assessed with the Agilent 2100 Bioanalyzer (Agilent Technologies). Equal amounts of DNA-*free* RNA (200 ng) were reverse-transcribed with the SuperScript IV First-Strand Synthesis System (Thermo Fischer Scientific) according to the conditions suggested by the manufacturer. RT–qPCR was performed to assess the expression of *CHI3L2* (Hs00970220_m1) with 1 ng of diluted complementary DNA and TaqMan 2X Universal PCR Master Mix (Thermo Fisher Scientific). Gene expression levels were calculated using the ΔCt method and 18S (Hs 99999901_s1) as normalizer. QuantStudio 5 (Thermo Fisher Scientific) and built-in proprietary software were used for data collection.

Suppression assays

CellTrace-labeled responder naive CD4$^+$ or CD8$^+$ T cells from healthy donors were cocultured with different effector to target (responder/suppressor) ratios with unlabeled CD127$^-$CD25$^-$CCR5$^+$CD27$^+$CD4$^+$ (Tr1-like) or CD127$^-$CD25$^+$ (FOXP3$^+$ T_{reg}) cells sorted from tumor-infiltrating lymphocytes of patients with CRC or NSCLC or peripheral blood from healthy donors using FACSAria II (BD Biosciences) in the presence of Dynabeads T-Activator CD3/CD28 (catalog no. 11131D; Thermo Fisher Scientific) at a bead-to-cell ratio of 1:10. Unlabeled naive CD4$^+$ T cells, CD4$^+$CCR5$^-$IL-7R$^-$ T_{eff} cells and CCR6$^+$IL$^-$7R$^+$ helper T cells were tested for suppressive capacities as control. Proliferation was assessed after 96 h. To assess the effect of PD1 block on the suppression of antigen-experienced CD8$^+$ T cells, fluorescence-activated cell sorting-purified CellTrace-labeled memory (CD45RA$^-$) T cells were stimulated with allogenic CD1c$^+$ dendritic cells and unlabeled EOMES$^+$ T_{reg} cells at a 1:1 ratio in the absence or presence of blocking anti-PD1 antibodies (10 µg ml^{-1}; clone J116 functional grade; eBioscience). Proliferation of CD8$^+$-gated T cells was assessed after 5 d.

In vitro induction of EOMES expression

Purified IL-7R$^-$CD25$^+$ T_{reg} cells or conventional antigen-experienced T cell subsets, that is, follicular helper T (T_{FH}) (IL-7R$^+$CXCR5$^+$), T_H1 (IL-7R$^+$CXCR3$^+$CCR6$^-$CXCR5$^-$CCR5$^-$), T_H17 (IL-7R$^+$CCR6$^+$ CXCR3$^-$CXCR5$^-$CCR5$^-$) or T_H2 (IL-7R$^+$CCR4$^+$CXCR3$^-$CCR6$^-$CXCR5$^-$) cells were stimulated with immobilized anti-CD3 antibodies (2 µg ml^{-1}) in the absence or presence of anti-CD28 antibodies and of 10 ng ml^{-1} of recombinant IL-4 or IL-12 or IL-27. After 7 d, viable CD4$^+$ T cells were analyzed for EOMES protein induction. Fold induction was calculated by normalizing EOMES expression on CD3/28-stimulated T_H1 cells in the absence of cytokines. EOMES induction in total

$CD4^+$ memory T cells was also compared in response to anti-CD3 antibodies, immature dendritic cells or lipopolysaccharide/R848-stimulated allogenic $CD1c^+$ dendritic cells in the absence or presence of IL-4.

Immunofluorescence

CRC and the relative nonneoplastic counterpart tissues (n = 3) were treated in a sucrose gradient and then embedded in optimal cutting temperature compound (Calbiochem). Sections were washed in PBS and incubated in blocking solution (PBS plus 10% normal goat serum; Vector Laboratories). Sections were incubated overnight at 4 °C with the following primary antibodies: anti-CD4, 5 μg μl^{-1} clone VIT4 (catalog no. 130-094-153; Miltenyi Biotec); anti-GZMK, 4,5 μg μl^{-1} (clone GM6C3); anti-EOMES, 10 μg μl^{-1} (clone WD1928). Sections were then washed and stained with isotype-specific secondary antibodies conjugated with Alexa Fluor dyes at 1:2,000 dilution (Alexa Fluor 488 goat anti-mouse IgG1, AF594 goat anti-mouse IgG2a, AF647 goat anti-mouse IgG2b; Thermo Fisher Scientific) for 1 h at 25 °C, followed by nuclear counterstaining with 4,6-diamidino-2-phenylindole (DAPI) (Thermo Fisher Scientific). Sections were mounted in 1,4-diazabicyclo[2.2.2]octane (DABCO) mounting medium (Sigma-Aldrich) and imaged using a multifunctional high-content analysis-automated Nikon Ti-E inverted widefield microscope, equipped with Crest Optics Video Confocal SuperResolution module and 16-light-emitting diode excitation device (pE-4000; CoolLED) for multiparametric fluorescence detection. At least n = 4 fields of view were acquired for each sample using a 100× total internal reflection fluorescence oil immersion objective (numerical aperture 1.46) and a 40× air objective (numerical aperture 0.9; both from Nikon Instruments) in large-scanning field modality to detect whole sections. Acquired images were processed and segmented using NIS-Elements v.5.02 (laboratory imaging software; Nikon Instruments) specific modules.

High-dimensional flow cytometry

Frozen samples were thawed in Roswell Park Memorial Institute 1640 supplemented with 10% FCS (Sigma-Aldrich), 1% penicillin-streptomycin and 1% ultra-glutamine (both from Lonza Bioscience) and 20 μg ml^{-1} deoxyribonuclease I from bovine pancreas (Sigma-Aldrich). After extensive washing with PBS (Sigma-Aldrich), cells were stained immediately with the Zombie Aqua Fixable Viability Kit (BioLegend) for 15 min at 25 °C. Then, cells were washed and stained with a combination of monoclonal antibodies purchased from either BD Biosciences, BioLegend, Santa Cruz Biotechnology or eBioscience. Monoclonal antibodies were previously titrated to define their optimal concentration, as described by Brummelman et al.[55]. Chemokine receptors were stained for 20 min at 37 °C, while all other surface markers (except for CD3) were stained for 20 min at 25 °C. Intracellular molecules (including CD3) were detected after fixation of cells with the FOXP3/transcription factor staining buffer set (eBioscience) according to the manufacturer's instructions and by incubating with specific monoclonal antibodies for 30 min at 4 °C.

Samples were acquired on a FACSymphony A5 flow cytometer (BD Biosciences) with proprietary software. Flow cytometry data were compensated in FlowJo v10 (FlowJo LLC) by using single-stained controls (BD CompBeads incubated with fluorescently conjugated antibodies), as described by Lugli et al.[56]. The following antibodies were used: anti-GZMK PE (clone GM6C3) 1:160; anti-GNLY Alexa Fluor 488 (clone RB1; BD Biosciences) 1:20; anti-CD25 Brilliant Violet 711 (clone BC96; BioLegend) 1:40; anti-FOXP3 PE-Cy5.5 (clone PCH101; eBioscience) 1:80; anti-CCR5 APC-Cy7 (clone 2DT/CCR5; BD Biosciences) 1:80; anti-PD1 Brilliant Violet 480 (clone EH12.1; BD Biosciences) 1:40; and anti-EOMES PE-eFluor610 (clone WD1928) 1:80.

Kaplan–Meier and multivariate analysis

Log-rank tests and Kaplan–Meier survival plots were used to evaluate the correlation (association) between patient survival time and expression of the *CHI3L2* gene. Transcriptional profiles and clinical parameters for patients with CRC (GSE17536, n = 177) and patients with NSCLC (GSE41271, n = 80) were downloaded from the Gene Expression Omnibus data portal. The melanoma dataset and corresponding clinical data were downloaded from The Cancer Genome Atlas database (skin cutaneous melanoma, n = 103). To correct for the effect of T cell amount within each sample, the expression of the selected gene was normalized to *CD3* gene expression (geometric mean of *CD3D*, *CD3E* and *CD3G*). To analyze the prognostic value of *CHI3L2*, cohorts were dichotomized into higher (gene level higher than the cutoff point, upper extreme) and lower groups (gene level lower than the cutoff point, lower extreme) whereas patients with the relative expression

between the two extremes were excluded from the survival analysis. The median of relative expression plus (minus) 5% MAD was used as a cutoff point for the dichotomization of patients into the two groups. Multivariate Cox proportional hazards analysis was performed to determine whether *CHI3L2* was an independent predictor of patient survival. For each dataset, a model with gene expression group and other covariates including sex, age and cancer stage was built. The hazard ratio and 95% confidence interval were estimated; only covariates with $P \leq 0.05$ were deemed as statistically significant. Statistical analysis was performed using the R survival package v3.2.3.

Data availability

Single-cell RNA-seq and TCR sequencing data that support the findings of this study have been deposited in the ArrayExpress archive under accession no. E-MTAB-7006. Gene lists derived from differential expression analysis and refined GSEA gene lists are available in the supplementary table files. All data generated during the current study are available from the corresponding authors upon request. Source data are provided with this paper.

References

1. Dobrzanski, M. J. Expanding roles for CD4 T cells and their subpopulations in tumor immunity and therapy. *Front. Oncol.* **3**, 63 (2013).
2. Shang, B., Liu, Y., Jiang, S.-J. & Liu, Y. Prognostic value of tumor-infiltrating FoxP3$^+$ regulatory T cells in cancers: a systematic review and meta-analysis. *Sci. Rep.* **5**, 15179 (2015).
3. Burzyn, D. et al. A special population of regulatory T cells potentiates muscle repair. *Cell* **155**, 1282–1295 (2013).
4. Cipolletta, D. et al. PPAR-γ is a major driver of the accumulation and phenotype of adipose tissue T_{reg} cells. *Nature* **486**, 549–553 (2012).
5. Sefik, E. et al. Individual intestinal symbionts induce a distinct population of RORγ$^+$ regulatory T cells. *Science* **349**, 993–997 (2015).
6. Fontenot, J. D., Gavin, M. A. & Rudensky, A. Y. Foxp3 programs the development and function of CD4$^+$CD25$^+$ regulatory T cells. *Nat. Immunol.* **4**, 330–336 (2003).
7. Tanaka, A. & Sakaguchi, S. Regulatory T cells in cancer immunotherapy. *Cell Res.* **27**, 109–118 (2017).
8. Häringer, B., Lozza, L., Steckel, B. & Geginat, J. Identification and characterization of IL-10/IFN-γ-producing effector-like T cells with regulatory function in human blood. *J. Exp. Med.* **206**, 1009–1017 (2009).
9. Pot, C. et al. Cutting edge: IL-27 induces the transcription factor c-Maf, cytokine IL-21, and the costimulatory receptor ICOS that coordinately act together to promote differentiation of IL-10-producing Tr1 cells. *J. Immunol.* **183**, 797–801 (2009).
10. Zhang, P. et al. Eomesodermin promotes the development of type 1 regulatory T (T_R1) cells. *Sci. Immunol.* **2**, eaah7152 (2017).
11. Gagliani, N. et al. Coexpression of CD49b and LAG-3 identifies human and mouse T regulatory type 1 cells. *Nat. Med.* **19**, 739–746 (2013).
12. Gruarin, P. et al. Eomesodermin controls a unique differentiation program in human IL-10 and IFN-γ coproducing regulatory T cells. *Eur. J. Immunol.* **49**, 96–111 (2019).
13. Mascanfroni, I. D. et al. Metabolic control of type 1 regulatory T cell differentiation by AHR and HIF1-α. *Nat. Med.* **21**, 638–646 (2015).
14. Roncarolo, M. G., Gregori, S., Bacchetta, R., Battaglia, M. & Gagliani, N. The biology of T regulatory type 1 cells and their therapeutic application in immune-mediated diseases. *Immunity* **49**, 1004–1019 (2018).

15. Dobrzanski, M. J. et al. Immunotherapy with IL-10- and IFN-γ-producing CD4 effector cells modulate 'Natural' and 'Inducible' CD4 TReg cell subpopulation levels: observations in four cases of patients with ovarian cancer. *Cancer Immunol. Immunother.* **61**, 839–854 (2012).

16. Marshall, N. A. et al. Immunosuppressive regulatory T cells are abundant in the reactive lymphocytes of Hodgkin lymphoma. *Blood* **103**, 1755–1762 (2004).

17. Pedroza-Gonzalez, A. et al. Tumor-infiltrating plasmacytoid dendritic cells promote immunosuppression by Tr1 cells in human liver tumors. *Oncoimmunology* **4**, e1008355 (2015).

18. Fan, X. & Rudensky, A. Y. Hallmarks of tissue-resident lymphocytes. *Cell* **164**, 1198–1211 (2016).

19. Stubbington, M. J. T., Rozenblatt-Rosen, O., Regev, A. & Teichmann, S. A. Single-cell transcriptomics to explore the immune system in health and disease. *Science* **358**, 58–63 (2017).

20. Azizi, E. et al. Single-cell map of diverse immune phenotypes in the breast tumor microenvironment. *Cell* **174**, 1293–1308.e36 (2018).

21. Guo, X. et al. Global characterization of T cells in non-small-cell lung cancer by single-cell sequencing. *Nat. Med.* **24**, 978–985 (2018).

22. Tirosh, I. et al. Dissecting the multicellular ecosystem of metastatic melanoma by single-cell RNA-seq. *Science* **352**, 189–196 (2016).

23. Zheng, C. et al. Landscape of infiltrating T cells in liver cancer revealed by single-cell sequencing. *Cell* **169**, 1342–1356.e16 (2017).

24. Torre, L. A. et al. Global cancer statistics, 2012. *CA Cancer J. Clin.* **65**, 87–108 (2015).

25. Webber, W. M. A., & Zobel, J. A similarity measure for indefinite rankings. *ACM Trans. Inf. Syst.* **28**, 20 (2010).

26. De Simone, M. et al. Transcriptional landscape of human tissue lymphocytes unveils uniqueness of tumor-infiltrating T regulatory cells. *Immunity* **45**, 1135–1147 (2016).

27. Plitas, G. et al. Regulatory T cells exhibit distinct features in human breast cancer. *Immunity* **45**, 1122–1134 (2016).

28. Togashi, Y., Shitara, K. & Nishikawa, H. Regulatory T cells in cancer immunosuppression—implications for anticancer therapy. *Nat. Rev. Clin. Oncol.* **16**, 356–371 (2019).

29. Alfen, J. S. et al. Intestinal IFN-γ-producing type 1 regulatory T cells coexpress CCR5 and programmed cell death protein 1 and downregulate IL-10 in the inflamed guts of patients with inflammatory bowel disease. *J. Allergy Clin. Immunol.* **142**, 1537–1547.e8 (2018).

30. Facciotti, F. et al. Evidence for a pathogenic role of extrafollicular, IL-10-producing $CCR6^{+}$B helper T cells in systemic lupus erythematosus. *Proc. Natl Acad. Sci. USA* **117**, 7305–7316 (2020).

31. Zhang, L. et al. Lineage tracking reveals dynamic relationships of T cells in colorectal cancer. *Nature* **564**, 268–272 (2018).

32. Keller, M. D. et al. T-cell receptor sequencing demonstrates persistence of virus-specific T cells after antiviral immunotherapy. *Br. J. Haematol.* **187**, 206–218 (2019).

33. Areshkov, P. O., Avdieiev, S. S., Balynska, O. V., Leroith, D. & Kavsan, V. M. Two closely related human members of chitinase-like family, CHI3L1 and CHI3L2, activate ERK1/2 in 293 and U373 cells but have the different influence on cell proliferation. *Int. J. Biol. Sci.* **8**, 39–48 (2012).

34. Lee, H.-O. et al. Lineage-dependent gene expression programs influence the immune landscape of colorectal cancer. *Nat. Genet.* **52**, 594–603 (2020).

35. Sato, M. et al. Human lung epithelial cells progressed to malignancy through specific oncogenic manipulations. *Mol. Cancer Res.* **11**, 638–650 (2013).

36. Smith, J. J. et al. Experimentally derived metastasis gene expression profile predicts recurrence and death in patients with colon cancer. *Gastroenterology* **138**, 958–968 (2010).

37. Petitprez, F., Meylan, M., de Reyniès, A., Sautès-Fridman, C. & Fridman, W. H. The tumor microenvironment in the response to immune checkpoint blockade therapies. *Front. Immunol.* **11**, 784 (2020).

38. Liu, D. et al. Integrative molecular and clinical modeling of clinical outcomes to PD1 blockade in patients with metastatic melanoma. *Nat. Med.* **25**, 1916–1927 (2019).

39. Roncarolo, M. G. et al. Interleukin-10-secreting type 1 regulatory T cells in rodents and humans. *Immunol. Rev.* **212**, 28–50 (2006).

40. Del Prete, G. et al. Human IL-10 is produced by both type 1 helper (Th1) and type 2 helper (Th2) T cell clones and inhibits their antigen-specific proliferation and cytokine production. *J. Immunol.* **150**, 353–360 (1993).

41. Zielinski, C. E. et al. Pathogen-induced human T_H17 cells produce IFN-γ or IL-10 and are regulated by IL-1β. *Nature* **484**, 514–518 (2012).

42. Gagliani, N. et al. T_H17 cells transdifferentiate into regulatory T cells during resolution of inflammation. *Nature* **523**, 221–225 (2015).

43. Ali, N. et al. Regulatory T cells in skin facilitate epithelial stem cell differentiation. *Cell* **169**, 1119–1129.e11 (2017).

44. Bluestone, J. A., Mackay, C. R., O'Shea, J. J. & Stockinger, B. The functional plasticity of T cell subsets. *Nat. Rev. Immunol.* **9**, 811–816 (2009).

45. Sakaguchi, S., Vignali, D. A. A., Rudensky, A. Y., Niec, R. E. & Waldmann, H. The plasticity and stability of regulatory T cells. *Nat. Rev. Immunol.* **13**, 461–467 (2013).

46. Alvisi, G. et al. IRF4 instructs effector Treg differentiation and immune suppression in human cancer. *J. Clin. Invest.* **130**, 3137–3150 (2020).

47. Brummelman, J. et al. High-dimensional single cell analysis identifies stem-like cytotoxic $CD8^+$ T cells infiltrating human tumors. *J. Exp. Med.* **215**, 2520–2535 (2018).

48. Galletti, G. et al. Two subsets of stem-like $CD8^+$ memory T cell progenitors with distinct fate commitments in humans. *Nat. Immunol.* **21**, 1552–1562 (2020).

49. Kzhyshkowska, J., Yin, S., Liu, T., Riabov, V. & Mitrofanova, I. Role of chitinase-like proteins in cancer. *Biol. Chem.* **397**, 231–247 (2016).

50. Libreros, S. & Iragavarapu-Charyulu, V. YKL-40/CHI3L1 drives inflammation on the road of tumor progression. *J. Leukoc. Biol.* **98**, 931–936 (2015).

51. Wolf, F. A., Angerer, P. & Theis, F. J. SCANPY: large-scale single-cell gene expression data analysis. *Genome Biol.* **19**, 15 (2018).

52. McCarthy, D. J., Campbell, K. R., Lun, A. T. L. & Wills, Q. F. Scater: pre-processing, quality control, normalization and visualization of single-cell RNA-seq data in R. *Bioinformatics* **33**, 1179–1186 (2017).

53. Becht, E. et al. Dimensionality reduction for visualizing single-cell data using UMAP. *Nat. Biotechnol.* **37**, 38–44 (2019).

54. Subramanian, A. et al. Gene set enrichment analysis: a knowledge-based approach for interpreting genome-wide expression profiles. *Proc. Natl Acad. Sci. USA* **102**, 15545–15550 (2005).

55. Brummelman, J. et al. Development, application and computational analysis of high-dimensional fluorescent antibody panels for single-cell flow cytometry. *Nat. Protoc.* **14**, 1946–1969 (2019).

56. Lugli, E., Zanon, V., Mavilio, D. & Roberto, A. FACS analysis of memory T lymphocytes. *Methods Mol. Biol.* **1514**, 31–47 (2017).

Acknowledgements

We thank M. Fakiola for discussions and critical revision of the manuscript, M. Moro and M. Crosti for technical assistance with cell sorting at Istituto Nazionale Genetica Molecolare and F. Colombo (Humanitas Flow Cytometry Core) for help with the FACSymphony A5 instrument setup. This work was supported by Associazione Italiana per la Ricerca sul Cancro (AIRC) grant no. IG2016-ID18575, AIRC grant no. IG2019-ID 23826 and Fondazione AIRC under 5 per mille 2019 - ID 22759 program to M. Pagani; Cancer Research UK Accelerator Award no. 22794, Fondazione AIRC under 5 per mille 2018 - ID 21147 to S.A.; 21091 program to S.A., A.B. and S.S.; AIRC grant no. IG2017 - ID 20676 to E.L.; AIRC grant no. IG2018-ID21923 to A.B.; AIRC grant nos. IG2015-ID17448 and IG2019-ID23581 to J.G.; and by an unrestricted grant of the Fondazione Romeo ed Enrica Invernizzi. J.B. is a recipient of the Fondo di Beneficenza Intesa San Paolo fellowship from AIRC. E.M.C.M. is a recipient of the 2017 Fondazione Umberto Veronesi postdoctoral fellowship. Purchase of the FACSymphony A5 (BD Biosciences) has been in part defrayed by a grant from the Italian Ministry of Health (agreement no. 82/2015).

Contributions

R.J.P.B., G.R., E.L., M.D.S., P.G. and J.B. designed and performed the main experiments, analyzed the data, performed the bioinformatics analyses and contributed to the preparation of the manuscript. L.D., M. Passaro, F.G., V.R., S.M. and E.M.C.M. contributed to setting up all the bioinformatics pipelines. C.D., S.O., C.G. and C.C. performed the immunofluorescence analyses. S.C., R. Bason, Y.S., E.C., R. Bosotti, G.D., M.L.S., M.M., V.B., M.L. and G.A. contributed to the tumor sample processing and analysis. A.S.-B., A.A., D.P., E.B., G.V., M.A., P.N., A.G., N.Z., E.O., A.P.C., N.M. and S.S. coordinated the clinical contributions and pathology analyses. S.B. and A.B. discussed the results, provided advice and commented on the manuscript. R.J.P.B., E.L., G.R., J.G., S.A. and M. Pagani wrote the manuscript. J.G., A.L., S.A. and M. Pagani designed the study and supervised the research. All authors discussed and interpreted the results.

Competing interests

M. Pagani and S.A. are members of the board of directors and stakeholders of CheckmAb. E.L. has a consulting agreement with Achilles Therapeutics. All other authors declare no competing interests.

Figure 1: Identification of intratumoral CD4+ T cell subsets in NSCLC and CRC.

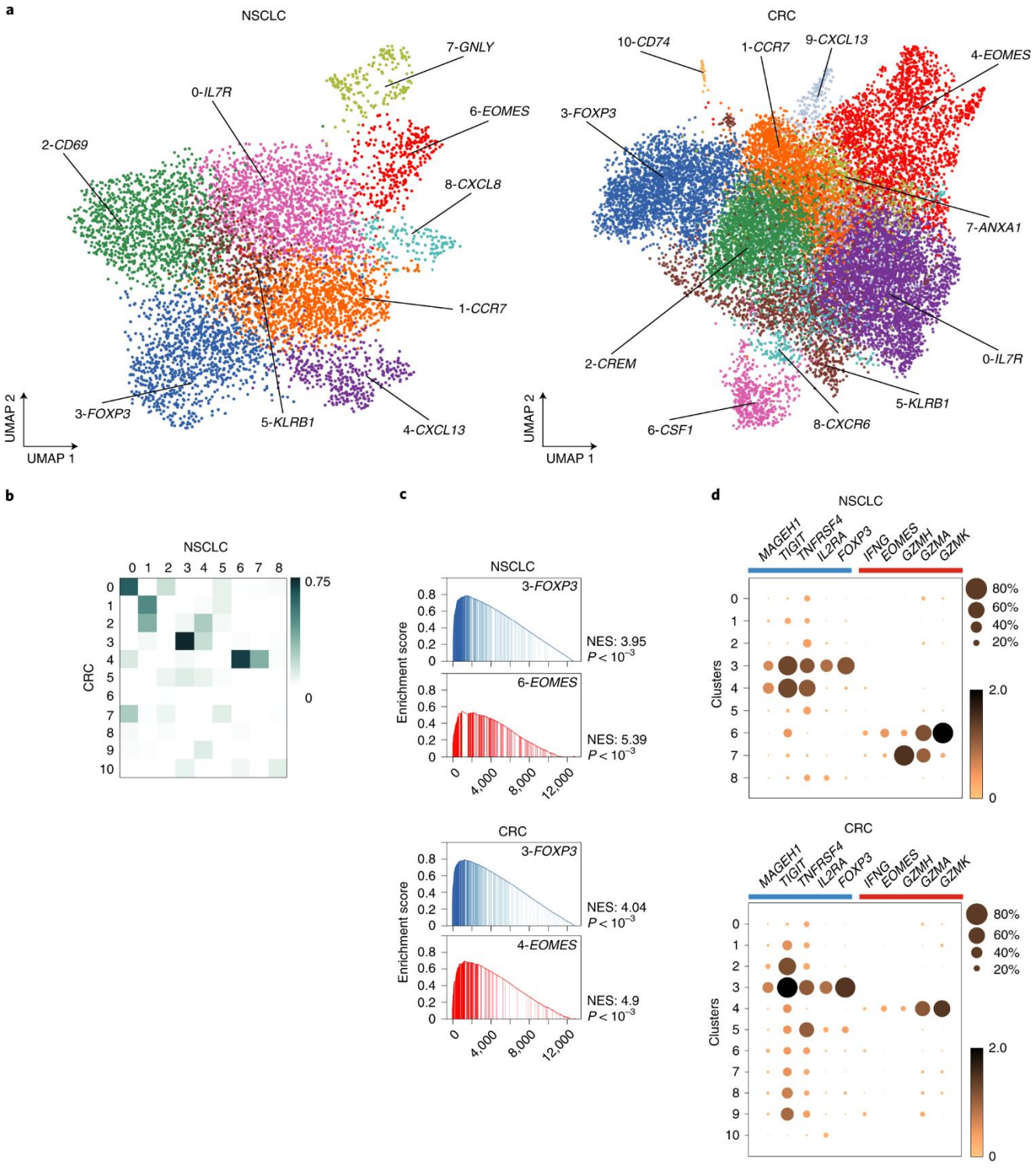

a, Unsupervised clustering of tumor-infiltrating CD4⁺ T cells. UMAP projection is used for data visualization. Each point depicts a single cell colored according to the clusters. Data represent the combined analysis of *n* = 2 NSCLC and *n* = 3 CRC samples **b**, Comparison of NSCLC and CRC clusters based on DEGs. The heatmap displays the cluster similarity calculated by rank-biased overlap. **c**, GSEA of reference CD4⁺ FOXP3⁺ (blue) and CD4⁺ EOMES⁺ (red) gene sets presented as enrichment score profiles with the normalized enrichment score (NES) and nominal *P* value. **d**, Expression and frequency of gene signatures for the FOXP3⁺ (blue) and EOMES⁺ (red) CD4⁺ subsets across the different CD4⁺ cell clusters.

Figure 2: EOMES⁺ GZMK⁺ CD4⁺ T cells with suppressive activity are highly enriched in different tumors.

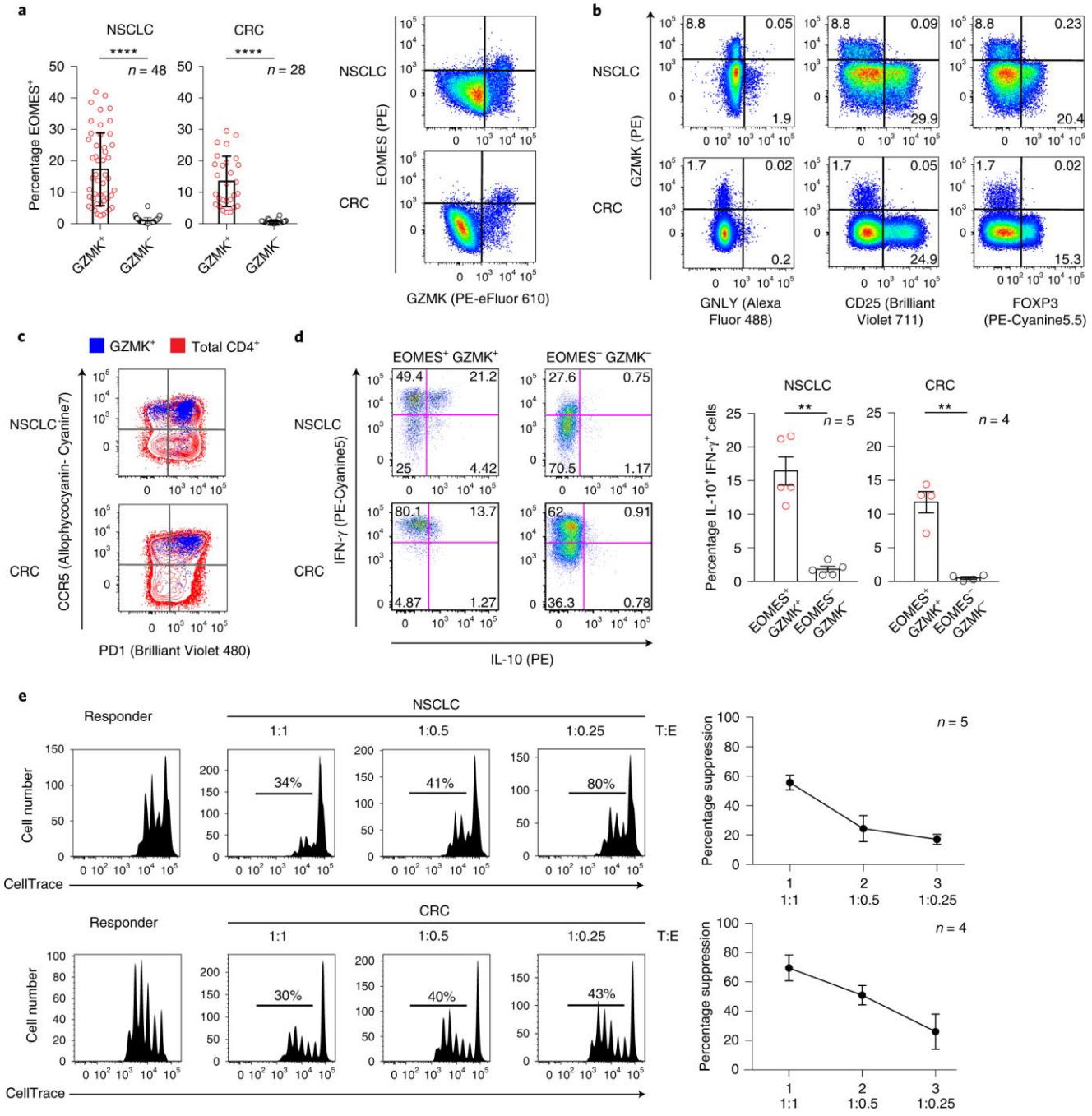

a, Percentage of EOMES⁺ cells among GZMK⁺ or GZMK⁻ CD4⁺ T cells infiltrating NSCLC ($n = 48$) or CRC ($n = 28$). Data are presented as mean values ± s.e.m. $^{****}P < 0.0001$ (two-tailed paired Wilcoxon test). One representative plot is shown in the right panel. **b**, GZMK⁺ Tr1-like cells lack GNLY, CD25 and FOXP3 expression. One representative experiment out of all NSCLC ($n = 48$) and CRC ($n = 28$) samples is shown. **c**, EOMES⁺ GZMK⁺ Tr1-like cells coexpress PD1 and CCR5. One representative experiment out of all NSCLC ($n = 48$) and CRC ($n = 28$) samples. **d**, Production of IL-10 and IFN-γ by EOMES⁺ GZMK⁺ and EOMES⁻GZMK⁻ CD4⁺ T cells after stimulation with PMA and ionomycin. $^{**}P < 0.01$ (two-tailed paired *t*-test). Exact *P* values are provided in the Souce Data. The bar plots show the mean values for $n = 5$ NSLC and $n = 4$ CRC samples ± s.e.m. **e**, Effector function of EOMES⁺ Tr1-like cells determined by the ability to suppress proliferation of conventional CD4⁺ T cells. The flow cytometry plots show the suppressive activity of EOMES⁺ CD4⁺ Tr1-like cells isolated from NSCLC or CRC tumors and cocultured with CellTrace-labeled EOMES⁻ CD4⁺ T cells activated with CD3/CD28 beads for 4 d. The percentages of proliferating cells are indicated. The capacity of EOMES⁺ CD4⁺ Tr1-like cells to suppress proliferation at different ratios is shown on the right. Data represent the mean values of $n = 5$ and $n = 4$ ± s.e.m. experiments performed with NSCLC- and CRC-infiltrating EOMES⁺ CD4⁺ Tr1-like cells.

Figure 3: Enrichment of FOXP3⁺ Treg and EOMES⁺ Tr1-like subsets in primary tumors and synchronous metastases.

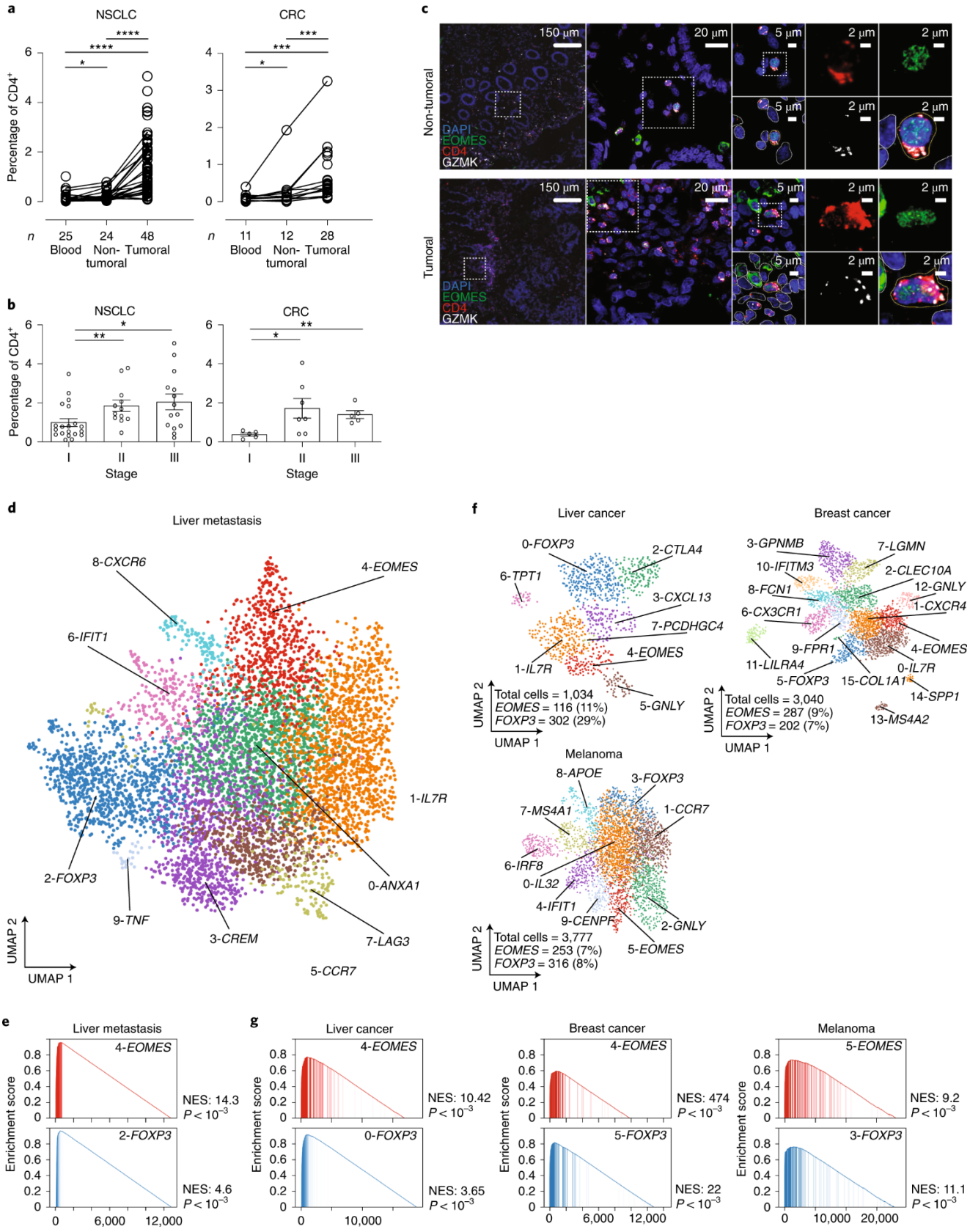

a, Frequencies of EOMES⁺ GZMK⁺ CD4⁺ T cells in paired samples of peripheral blood ($n = 25$), non-tumoral adjacent tissues ($n = 24$) and tumoral tissues from NSCLC ($n = 48$) and peripheral blood ($n = 11$), non-tumoral adjacent tissues ($n = 12$) and tumoral tissues ($n = 28$) from patients with CRC. The lines identify paired samples. $*P < 0.05$, $***P < 0.001$, $****P < 0.0001$ (two-tailed Wilcoxon test). Exact *P* values are provided in the Source Data. **b**, Bar plots representing the frequencies of EOMES⁺ GZMK⁺ CD4⁺ T cells in tumor

tissues at different disease stages (NSCLC: stage I, *n* = 20; stage II, *n* = 12; stage III, *n* = 14; CRC: stage I, *n* = 5; stage II, *n* = 7; stage III, *n* = 5). *$P < 0.05$, **$P < 0.01$ (two-tailed Mann–Whitney *U*-test). The exact *P* values are provided in the Source Data. **c**, Estimation of enrichment in intratumoral EOMES$^+$ Tr1-like cells by immunofluorescence. Multiple immunofluorescence labeling for CD4 (red), GZMK (white) and EOMES (green) in a representative paired non-tumoral colon (top) and CRC (bottom) sample. Zoomed-in insets show areas that are triple-positive for CD4. GZMK images at different magnification are shown. Cellular segmentation highlights the orange-labeled cell contours of triple-positive cells versus the white-labeled cell contours for all other segmented cells. **d**. Unsupervised clustering of CD4$^+$ T cell populations purified from two liver metastases synchronous to the primary CRC visualized in Fig. 1a. UMAP projection is used for data visualization. Each point depicts a single cell, colored according to the designated cluster. **e**, Enrichment score profiles of GSEA analyses of CD4$^+$ T cells from liver metastases synchronous to the CRC in Fig. 1a, performed using refined reference gene sets of tumor-infiltrating FOXP3$^+$ T_{reg} and EOMES$^+$ Tr1-like cells with NES and nominal *P* value. **f**, UMAP projection of liver, breast cancer and melanoma single-cell CD4$^+$ T cell datasets. The percentage of CD4$^+$ FOXP3$^+$ and EOMES$^+$ cells over total CD4$^+$ is shown for each tumor type. **g**, GSEA analyses of CD4$^+$ T cells from liver cancer, breast cancer and melanoma performed with refined reference gene sets of tumor-infiltrating FOXP3$^+$ T_{reg} and EOMES$^+$ Tr1-like cells. Results are shown as enrichment score profiles with NES and nominal *P* value.

Figure 4: Clonal expansion and clonotype sharing across CD4⁺ T cell subsets in primary and metastatic tumors.

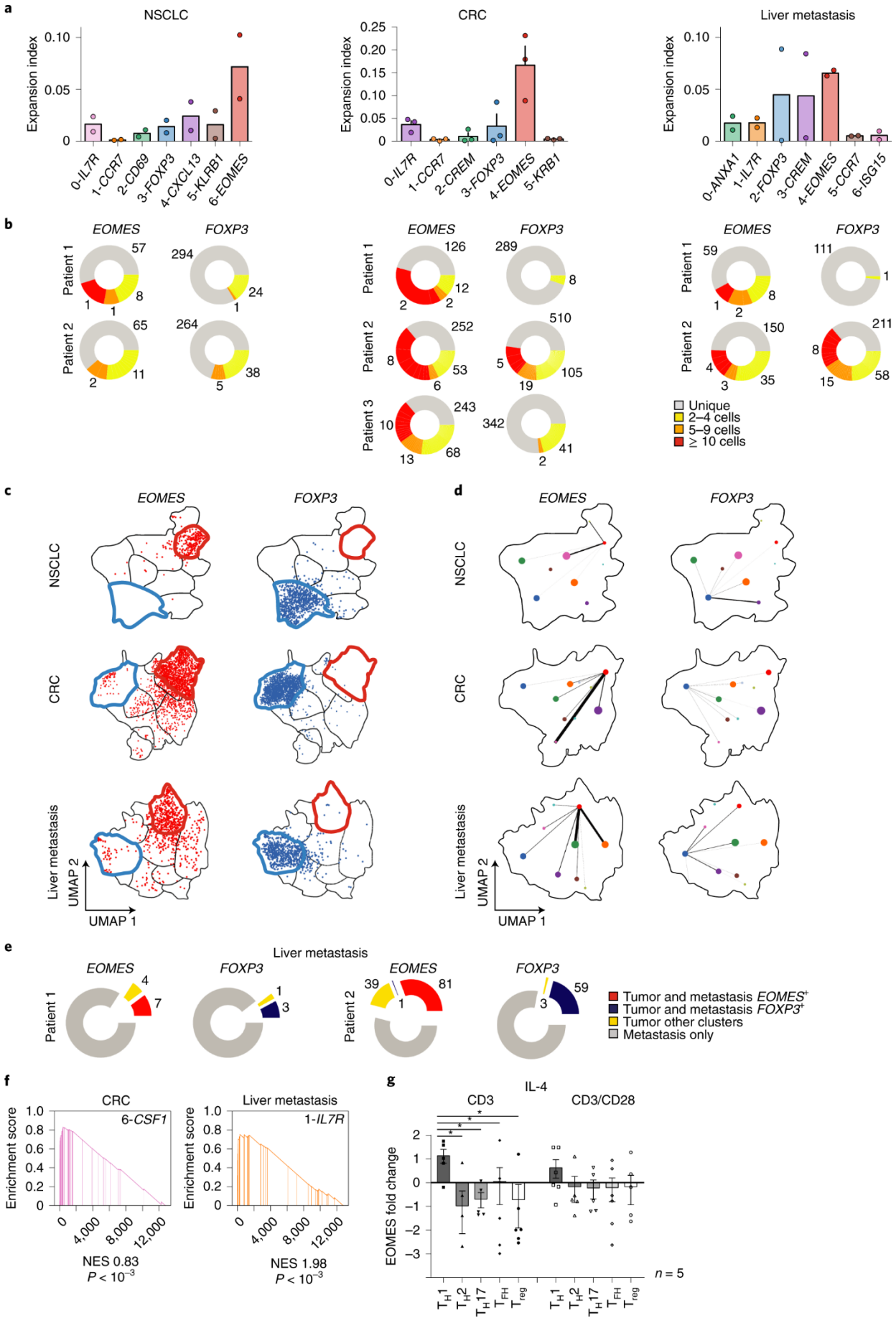

a, Clonal expansion index of $CD4^+$ T cell clusters as designated in the UMAP projection from *n* = 2 NSCLC and *n* = 3 CRC primary tumors shown in Fig.1a and from *n* = 2 CRC liver metastases in Fig. 3c. The bars in the CRC expansion index panel indicate the mean ± s.e.m. **b**, Pie charts showing the TCR clonal expansion of $FOXP3^+$ T_{reg} and $EOMES^+$ $CD4^+$ Tr1-like cells in NSCLC and CRC primary tumors and in synchronous liver metastases of CRCs. Clonal size is categorized by the number of cells with identical αβ TCR. The number of clones in each category is shown. **c**, Distribution of clonotypes found primarily in *FOXP3*$^+$ (blue) or *EOMES*$^+$ (red) subsets within all populations analyzed. Expanded clonotypes are shown irrespective of their size. **d**, Clonal overlap of *FOXP3*$^+$ and *EOMES*$^+$ cells across clusters, evaluated by Morisita's overlap index. Each node in the Morisita's overlap index graph stands for a cluster, with dot size proportional to cluster numerosity; line width is proportional to the pairwise TCR sharing between clusters. **e**, TCR clonotype sharing between primary and metastatic CRC. The pie charts represent clonotypes of $EOMES^+$ Tr1-like (red) and $FOXP3^+$ T_{reg} (blue) cells present in both primary tumors and synchronous metastases. Clonotypes shared between $FOXP3^+$ Treg or $EOMES^+$ Tr1-like and any other cluster from primary tumor and metastases are represented in yellow. TCR clonotypes present uniquely in metastases are shown in gray. The number of clones in each category is shown. **f**, GSEA analyses presented as enrichment score profiles of reference $CD4^+$ T_H1 gene set for CRC cluster 6 (pink plot) and liver metastasis cluster 1 (orange plot) with the NES and nominal *P* value. **g**, Induction of EOMES in purified T cell subsets on stimulation with anti-CD3 and IL-4 in the absence or presence of CD28 co-stimulation. $*P < 0.05$ (one-way analysis of variance (ANOVA) with Newman–Keuls correction for multiple comparisons). Data are presented in $\log_2$ scale as the mean of five experiments ± s.e.m.

Figure 5: Enrichment of intratumoral EOMES⁺ Tr1-like cells correlates with tumor progression and response to immunotherapy.

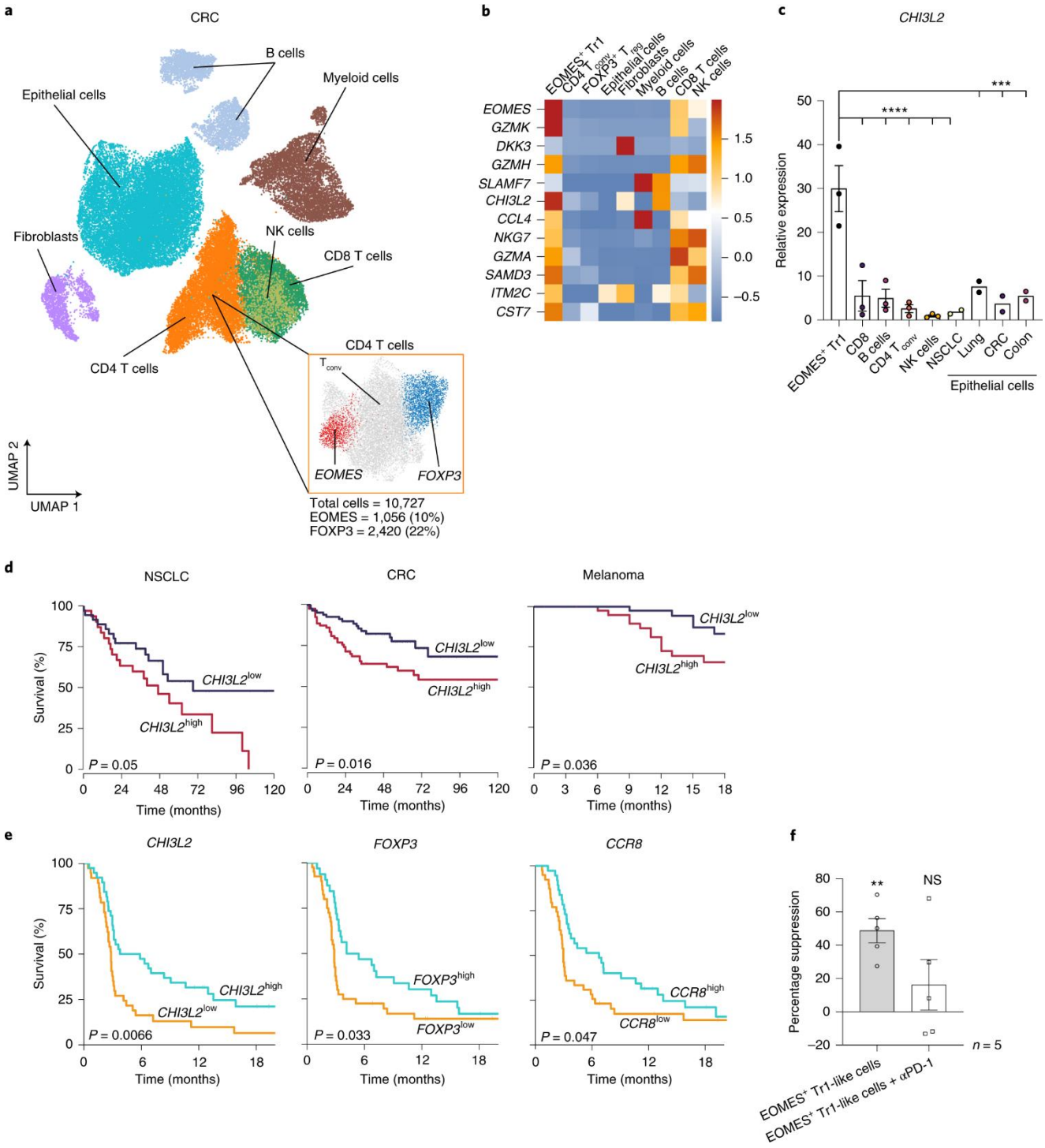

a, Unsupervised clustering of all cell types in CRC samples as determined by scRNA-seq data visualized with UMAP projection. Each point depicts a single cell, which is colored according to the clusters. Data represent the combined analysis of *n* = 23 CRC samples. The inset highlights *FOXP3*⁺ and *EOMES*⁺ subsets within the CD4⁺ T cell cluster. **b**, Heatmap representing the relative expression of the most specific markers for EOMES⁺ Tr1-like cells across all the populations identified through the combined analysis of *n* = 23 CRC scRNA-seq datasets. **c**, Relative expression, measured by RT–qPCR, of *CHI3L2* in tumor-infiltrating lymphocyte subsets, whole tumoral tissues (NSCLC or CRC) and paired non-tumoral lung and colon tissues depleted of the immune component. The bars represent the means of *n* = 3 ± s.e.m. for immune cells and *n* = 2 for epithelial cells. ****P* < 0.001, *****P* < 0.0001 *(*one-way ANOVA with Dunnett's correction versus EOMES⁺ Tr1-like cells as reference). Exact *P* values are provided in the Source Data. **d**, Kaplan–Meier plots used to compare CRC (*n* = 177), squamous NSCLC (*n* = 75) and melanoma (n = 103) survival; the intratumoral EOMES⁺ T cell signature transcript was normalized for the amount of T cells present (assessed as CD3 expression). Univariate analysis confirmed a significant difference in overall survival curve comparing patients with high and low expression of *CHI3L2*. Statistical significance was determined by two-tailed

log-rank test. **e**, Kaplan–Meier plots indicate the progression-free survival of patients with melanoma (*n* = 121) treated with anti-PD1. Patients were grouped according to the intratumoral expression of *CHI3L2*, *FOXP3* or *CCR8* before the initiation of treatment. Statistical significance was determined by two-tailed log-rank test. **f**, Suppression of antigen-experienced $CD8^+$ T cell proliferation by $EOMES^+$ Tr1-like cells in the absence (gray) or presence (white) of blocking anti-PD1 antibodies. $^{**}P < 0.01$, NS > 0.05 (two-tailed paired *t*-test performed for each condition versus antigen-experienced $CD8^+$ T cells cocoltured with $CD4^+$-naive T cells as controls). Exact *P* values are provided in the Source Data. The bars represent *n* = 5 independent experiments ± s.e.m. T_{conv}, conventional T cells.

Extended Data Fig. 1: Overview of the experimental workflow.

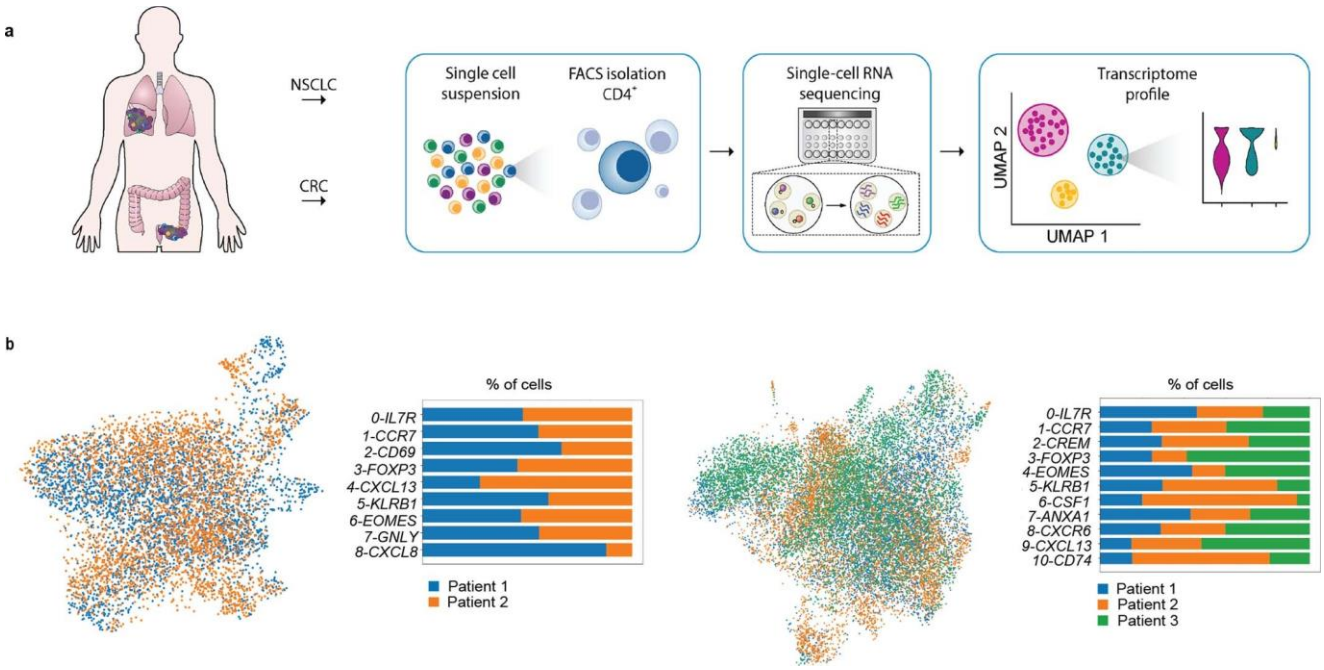

a, Schematic overview of the experimental workflow. **b**, Single cell analysis quality controls. UMAP projection for both NSCLC and CRC as in Fig. 1b colored according to patient identity. Bar plots represent the percentage of cell deriving related to each patient for NSCLC and CRC clusters.

Extended Data Fig. 2: Single-cell analysis on additional NSCLC and CRC samples.

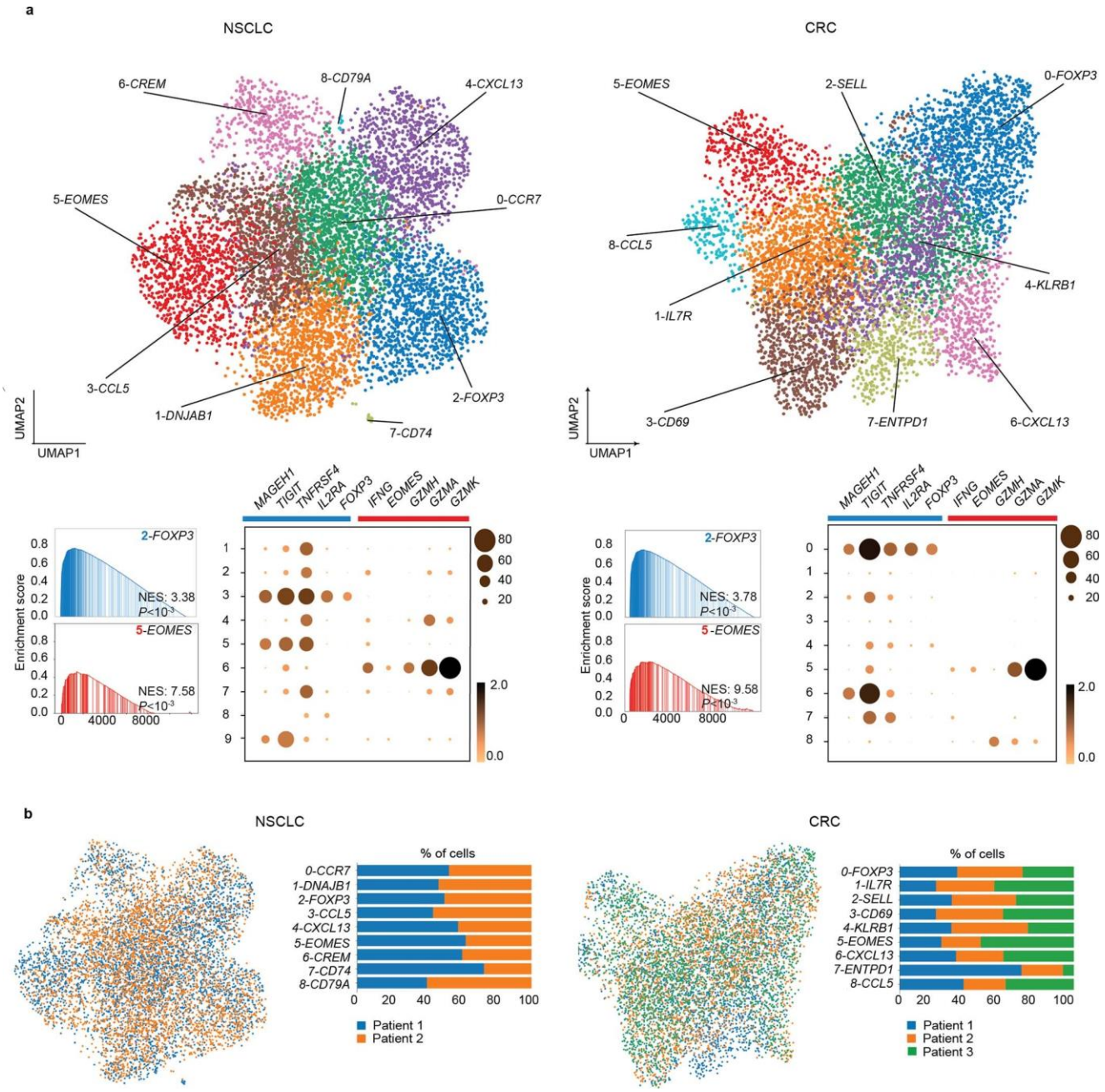

a, *Upper panel*: Unsupervised clustering of tumor infiltrating CD4⁺ T cells data generated with Chromium Single Cell 3' protocol, UMAP projection is used for data visualization. *Lower panel*: Gene set enrichment analyses of reference CD4⁺ FOXP3⁺ and CD4⁺ EOMES⁺ gene sets (blue and red) presented as enrichment score profiles with the normalized enrichment score (NES) and nominal *P*-value. Expression and frequency of CD4⁺ FOXP3⁺ and EOMES⁺ subset gene signatures (blue and red) are shown across the different CD4⁺ cell clusters. **b**, UMAP projection for both NSCLC and CRC generated with Chromium Single Cell 3' protocol colored according to patient identity. Bar plots the percentage of cell deriving related to each patient for NSCLC and CRC clusters.

Extended Data Fig. 3: Characterization of EOMES+ Tr-1 like cells.

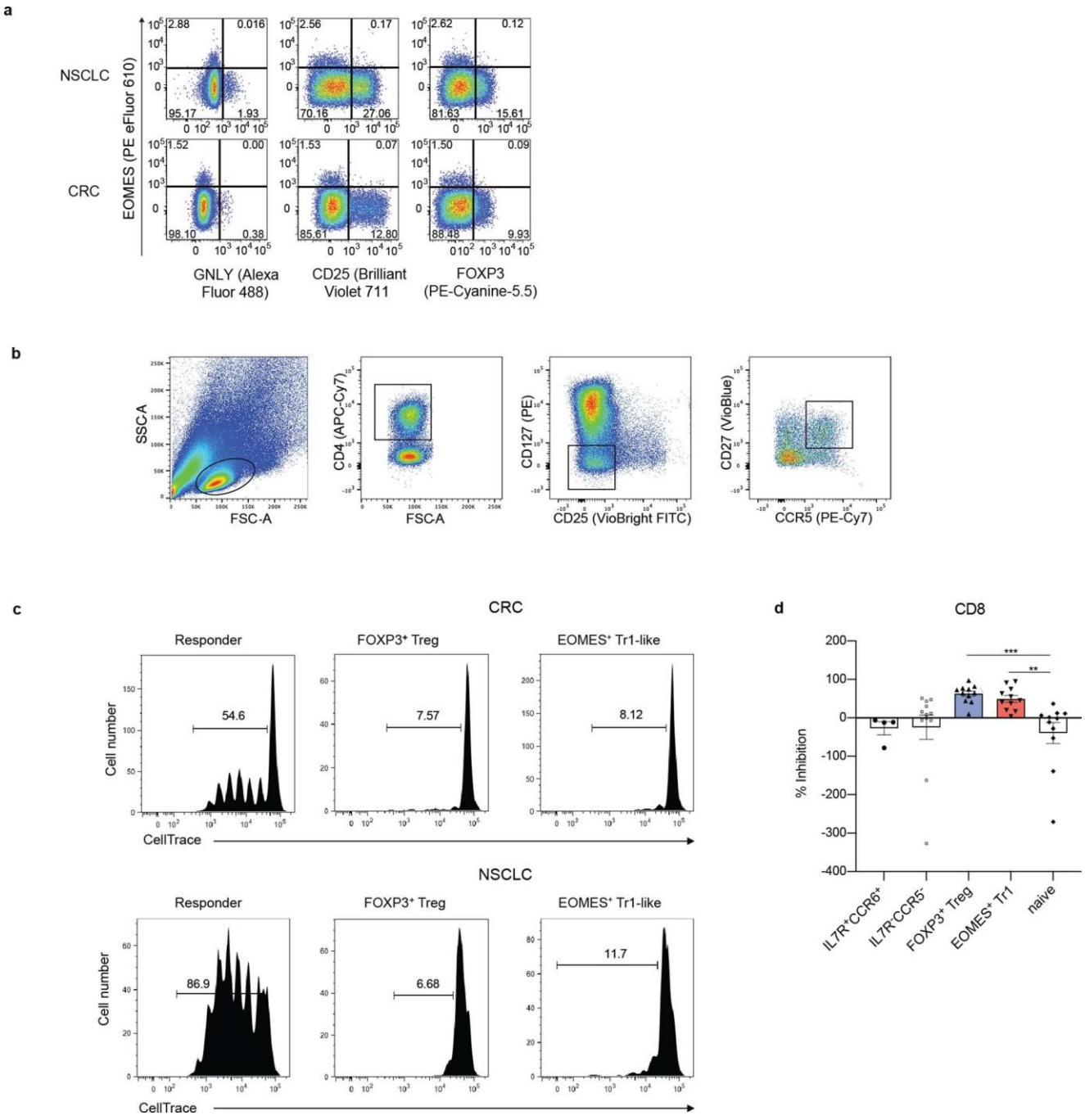

a, EOMES$^+$ Tr1-like cells lack GNLY, CD25 and FOXP3 expression. One representative experiment out of all NSCLC (n= 48) and CRC (n= 28) patients is shown. **b**, Tr1-like cell sorting strategy: CCR5$^+$CD27$^+$Tr1-like cells were purified from the CD4$^+$ fraction of CD127$^-$CD25$^-$ Tr1-containing cells by cell sorting. **c**, Representative flow cytometry plots showing suppressive activity of EOMES$^+$ Tr1-like cells *vs* FOXP3$^+$ Treg cells isolated from tumor samples (NSCLC or CRC). Percentage of proliferating cells is indicated. **d**, EOMES$^+$ Tr1-like cells and FOXP3$^+$ regulatory T-cells suppress CD8$^+$ T-cell proliferation. FACS- purified naïve CD8$^+$ T-cells were labelled with CellTrace and stimulated with anti-CD3/28 beads in the presence of CD4$^+$FOXP3$^+$ (n=12) EOMES$^+$ Tr1-like (n=11) subsets, naïve CD4$^+$ T-cells (n=11) conventional effector cells: CD127$^-$CD25$^-$CCR5$^-$CD4$^+$ (n=12) and CCR6$^+$CD127$^+$CD25$^-$CD4$^+$ cells containing IL-10 producing helper T-cells (n=4). **** P<0.001 **P<0.01 (*two-tailed unpaired t-test). Bars represent percentage of suppression ± s.e.m..Exact *P* values are provided in the Source Data.

Extended Data Fig. 4: TCR percentage and clonal size estimation.

a

NSCLC

5p_NSCLC_K		
Reconstructed TCR	Patient 1	Patient 2
α	47	47
αα	5	8
ααβ	231	121
αβ	2215	1597
β	262	450
ββ	5	29
ααββ	29	23
αββ	76	153
TCR+	2870	2428
Total	3508	3153
TCR-	638	725
	18%	23%

CRC

5p_CRC_K			
Reconstructed TCR	Patient 1	Patient 2	Patient 3
α	108	102	83
α α	6	14	9
ααβ	318	297	278
αβ	3665	2864	2916
β	606	533	580
ββ	16	25	36
ααββ	49	36	93
αββ	146	224	313
TCR+	4914	4095	4308
Total	6394	6029	6225
TCR-	1480	1934	1917
	23%	32%	31%

Liver Metastasis

5p_CRC_metastasis		
Reconstructed TCR	Patient 1	Patient 2
α	47	29
α α	6	2
ααβ	97	179
αβ	1081	1804
β	254	253
ββ	14	18
ααββ	1	105
αββ	47	235
TCR+	1547	2625
Total	2010	4479
TCR-	463	1854
	23%	41%

b

NSCLC

		Patient 1		Patient 2	
		EOMES	FOXP3	EOMES	FOXP3
N Cells	1	57	294	65	264
	2-4	20	53	28	81
	5-9	9	5	13	31
	>=10	18	0	0	0
N Clones	1	57	294	65	264
	2-4	8	24	11	38
	5-9	1	1	2	
	>=10	1	0	0	0

CRC

		Patient 1		Patient 2		Patient 3	
		EOMES	FOXP3	EOMES	FOXP3	EOMES	FOXP3
N Cells	1	126	289	252	510	243	342
	2-4	32	16	124	261	181	93
	5-9	13	0	33	119	88	11
	>=10	104	0	291	179	160	0
N Clones	1				510	243	342
	2-4	12	8	53		68	41
	5-9	2	0	6	19	13	2
	>=10	2	0	8	5	10	0

Liver Metastasis

		Patient 1		Patient 2	
		EOMES	FOXP3	EOMES	FOXP3
N Cells	1	59	111	150	211
	2-4	19	2	85	144
	5-9	14	0	20	95
	>=10	10	0	49	134
N Clones	1	59	111	150	211
	2-4	8	1	35	58
	5-9	2	0	3	15
	>=10	1	0	4	8

c

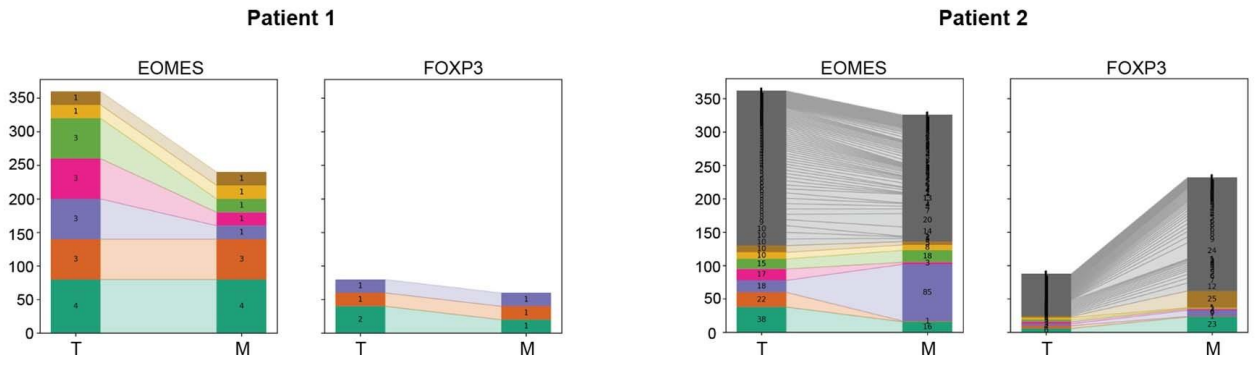

a, Number of α and β chains combinations identified by TCR-sequencing for each patient. **b**, Number of cells and number of clones for different clonal size (grey=unique; yellow=2-4; orange=5-9; red>10 clones) for each NSCLC and CRC patient. **c**, Number of cells for each EOMES$^+$ Tr1-like or FOXP3$^+$ Treg cell clone for both CRC primary tumor (T) and their synchronous liver metastasis (M).

Extended Data Fig. 5: EOMES induction and Tr1-like cell stability.

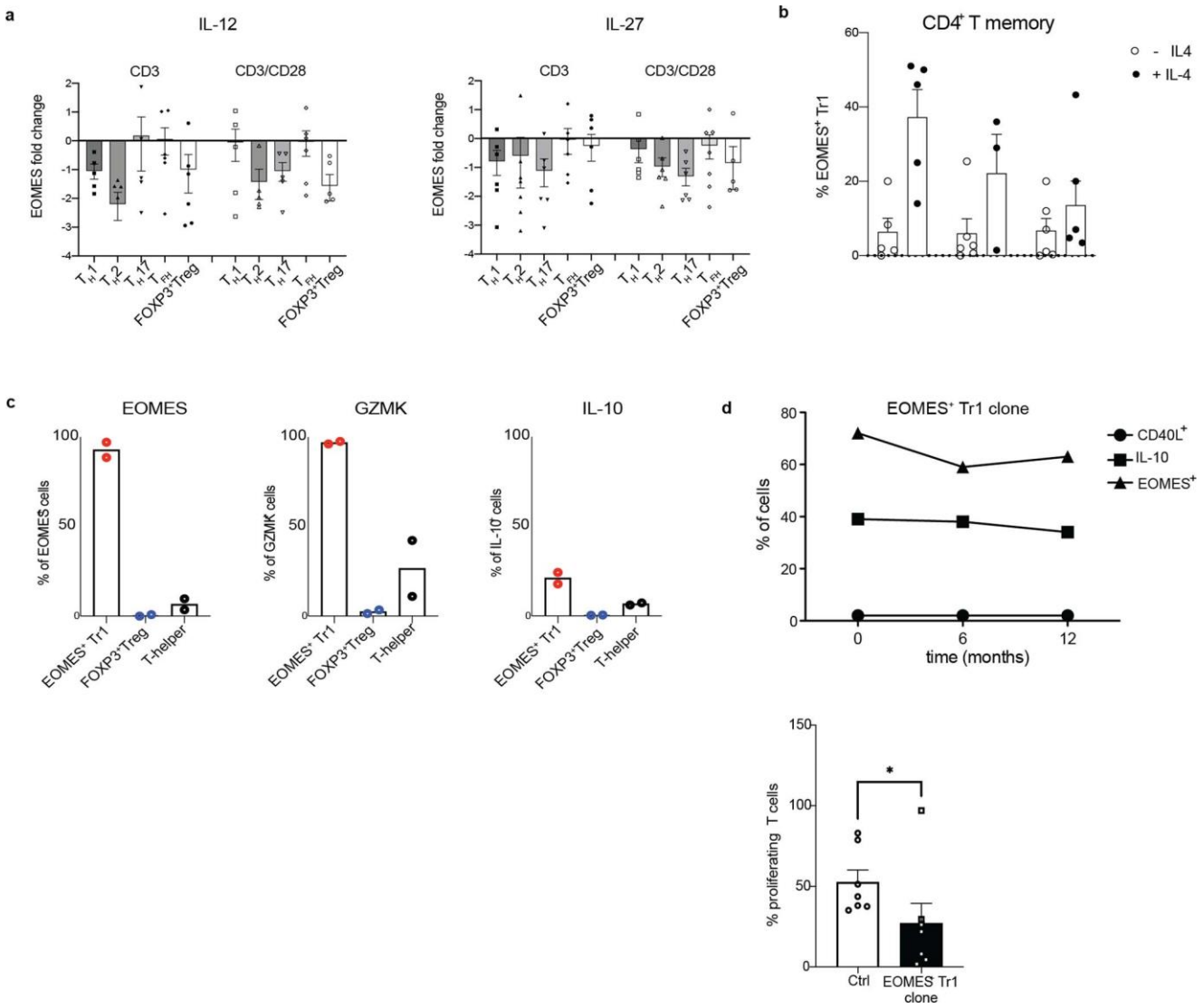

Induction of EOMES in purified T-cell subsets upon stimulation with anti-CD3 antibodies and IL-12 or IL-27 in the absence and presence of CD28 co-stimulation. Results are presented as means of 6 biological replicates ± s.e.m. **b**, Induction of EOMES in CD4$^+$ T memory cells upon stimulation with immobilized anti-CD3 antibodies, immature or mature CD1c$^+$DC in the presence (black dots) or absence (white dots) of IL-4. Results are presented as average of ≥ 3 experiments ± s.e.m.. **c**, Expression of EOMES, GZMK and IL-10 in CD4$^+$T-cell lines after 3 weeks of *in vitro* culture. T-cell subsets were sorted first ex vivo according to IL-7R and CD25 expression and then, after PMA/Ionomycin stimulation, according to IL-10 and CD40L expression with an IL-10 secretion assay. Bars represent means of n=2 biological replicates. **d**, *Upper panel*: EOMES, IL-10 and CD40L expression in a CD4 EOMES T-r1 clone at different time points: 3 weeks after generation (left) and after 6 (middle) or 12 months (right). *Lower panel*: Suppression of naïve CD4$^+$ T-cell proliferation by the same CD4$^+$EOMES$^+$ Tr1 clone means of n=7 biological replicates is shown *P< 0.05 (two-tailed paired t-test). Exact *P* values are provided in the Source Data.

Source Data Fig. 2

Fig.2e Suppressive activity of EOMES$^+$ CD4$^+$ Tr1-like

	Ratio	% of Suppression				
CRC	Rsponders/ EOMES$^+$ Tr1					
	1:1	82	79	72	44	
	1:0.5	67	51	48	39	
	1:0.25	48	37	11	6	
NSCLC						
	1:1	64	61	49	63	43
	1:0.5	58	14	15	27	11
	1:0.25	25	17	13	21	9

Source Data Fig. 3

Fig.3b % of EOMES$^+$GRZMK$^+$

CRC	stage I	stage II	stage III	**NSCLC**	stage I	stage II	stage III
	0,13	2,811	2,142		0,826	1,319	2,35
	0,499	1,156	1,46		2,497	1,854	0,42
	0,412	2,009	1,327		3,481	0,466	1,406
	0,249	1,177	0,967		0,527	3,787	2,674
	0,576	0,413	1,103		0,432	2,067	2,785
		0,406			0,543	2,388	1,898
		4,057			2,154	1,093	0,823
					0,125	3,652	0,21
	Exact Pvalue I vs II =0.048				1,947	1,178	3,626
	Exact Pvalue I vs III =0.0079				0,626	1,443	5,059
					0,375	1,692	4,459
					1,832	1,233	0,862
					0,349		0,686
					0,778		1,361
					0,101		
					0,398		
					0,933		
					0,798		
					0,779		
					0,318		
					Exact Pvalue I vs II =0.072		
					Exact Pvalue I vs III =0.0185		

Source Data Fig. 4

FIG.4a Expansion Index

NSCLC		**Cluster**						
	Patient	0	1	2	3	4	5	6
	1	0,009	0,001	0,004	0,008	0,010	0,003	0,102
	2	0,024	0,002	0,011	0,020	0,038	0,029	0,041
CRC		**Cluster**						
	Patient	0	1	2	3	4	5	
	1	0,019	0,001	0,001	0,002	0,231	0,003	
	2	0,048	0,005	0,026	0,085	0,179	0,005	
	3	0,042	0,005	0,003	0,012	0,089	0,006	
Liver Metastasis		**Cluster**						
	Patient	0	1	2	3	4	5	6
	1	0,011	0,022	0,001	0,003	0,068	0,005	0,000
	2	0,024	0,013	0,089	0,084	0,063	0,005	0,001

Source Data Fig. 5

Fig.5c Relative expression data of *CHI3L2* transcript									
	EOMES$^+$ Tr1	CD8	B cells	CD4 Tconv	NK	colon	CRC	lung	NSCLC
	39,623058	12,467266	2,252490	2,753535	0,611795	4,383486	1,916470	6,308882	2,324967
	21,499514	1,233227	9,009962	0,941747	0,837954	6,534790	5,486229	8,862977	1,401351
	28,805460	2,892396	3,677013	4,056210	1,435049				
	Dunnett's multiple comparisons test			Summary	Adjusted *P* Value				
	EOMES$^+$ Tr1 vs. CD8			****	<0.0001				
	EOMES$^+$ Tr1 vs. B cells			****	<0.0001				
	EOMES$^+$ Tr1 vs. CD4 Tconv			****	<0.0001				
	EOMES$^+$ Tr1 vs. NK			****	<0.0001				
	EOMES$^+$ Tr1 vs. colon			***	0,0003				
	EOMES$^+$ Tr1 vs. CRC			***	0,0001				
	EOMES$^+$ Tr1 vs. lung			***	0,0006				
	EOMES$^+$ Tr1 vs. NSCLC			****	<0.0001				

Source Data Extended Data Fig. 2

Extended_Data Fig.2d				
IL7R$^+$CCR6$^+$	**IL7R$^-$CCR5$^-$**	**FOXP3$^+$ Treg**	**EOMES$^+$ Tr1**	**naive**
-6,13	15,77	44,20	55,40	-1,32
-11,47	-6,30	56,79	45,23	-52,58
-12,47	-6,64	64,42	40,14	
-78,08	-162,10	64,52	63,42	-138,70
	47,81	41,20	16,71	12,01
	8,29	74,91	37,97	-27,79
	43,45	97,39	94,84	36,87
	30,38	72,60		6,49
	-326,71	71,14	19,88	-270,88
	-0,90	9,88	3,72	1,49
	11,97	77,38	91,00	-11,15
	50,83	81,75	74,58	11,13
P value FOXP3$^+$ Treg vs naive =0.0010				
P value EOMES$^+$ Tr1 vs naive =0.0055				

Source Data Extended Data Fig. 5

Extended Data Fig. 5d Suppression of naïve CD4+ T-cell proliferation by CD4$^+$EOMES$^+$ Tr1 clone		
Percentage of proliferating T cells		
Ctrl	EOMES$^+$ Tr1 clone	
37,5	21,9	
38,1	1,8	
35,2	4,5	
51,3	8,11	
78,8	97	
43,7	29,5	
83,1	26,3	
P value EOMES$^+$ Tr1 clone vs ctrl =0.032		